ABSTRACT

Title of Thesis:	DETECTING THE DEPTH OF THE CRACK BY LASER SPOT THERMOGRAPHY
	Niraj Jha, Master of Science, 2020
Thesis Directed By:	Professor Peter Chang, Civil and Environmental Engineering

Understanding the properties of the cracks can give detailed insight about the health and status of any structure. Some cracks may not be detrimental, others may cause the structure to collapse if not inspected, recognized and repaired ahead of time. This article is about detecting the depth of a crack using laser spot thermography. A 3D finite element analysis of a laser beam as a heat source and steel specimen with cracks of various depths is performed by using COMSOL Multiphysics 5.5. Then the relationship between the crack depth and the temperature differential index is studied by using a regression analysis. Finally, the equation obtained from the regression analysis is used to predict the depth of the arbitrary cracks. The predicted depth is verified with their actual depths. The results are accurate with the error ranging from +0.3 mm to -0.2 mm.

DETECTING THE DEPTH OF THE CRACK BY LASER SPOT THERMOGRAPHY

by

Niraj Jha

Thesis submitted to the Faculty of the Graduate School of the
University of Maryland, College Park, in partial fulfillment
of the requirements for the degree of
Master of Science
2020

Advisory Committee:
Professor Peter Chang, Chair
Professor Amde Amde
Professor Yunfeng Zhang

Acknowledgements

I would like to thank my advisor Professor Peter Chang for helping me during my thesis work. I would also like to thank Professor Mohammed Basheer Chalil for answering some of my queries related to his articles.

Table of Contents

Acknowledgements ii

Table of Contents iii

List of Tables iv

List of Figures v

List of Abbreviations vi

Chapter 1: Introduction 1

Chapter 2: Finite Element Modelling 5

Geometry: 5
Material Properties: 6

Heat Source and Heat Transfer in Solids: 6
Heat Source 6
Heat Transfer in Solids 7
Mesh 8

Study Settings 13

Model Calibration 14

Results from Finite Element Analysis 16

Chapter 3: Data Analysis 23

Data Collection from FEM Analysis 23

Regression Analysis 25

Chapter 4: Checking the Result for a Crack of Arbitrary Depth 28

Chapter 5: Conclusions 31

Appendix A 32

Appendix B 59

Bibliography 60

List of Tables

Table.1. Partition Domain & Mesh Control Domain 5
Table.2. Test Specimen and Crack after Extrude & Subtraction 6
Table.3. Parameter 1 6
Table.4. Variables 1 7
Table.5. Time Dependent Solver Settings 13
Table.6. Time Stepping Settings 14
Table.7. Comparison between Experimental and Simulation Results 15
Table.8. Location of Heat Source at 4 mm from the Crack 20
Table.9. Location of Heat Source 16 mm from the Crack 20
Table.10. Time(t') & Depth of the Crack 24
Table.11. Temperature Differential Index and Crack Depth (Actual depth used for regression & depth from the regression equation) 27
Table.12. The Heat Source Used while Modelling Arbitrary Cracks 28
Table.13. Predicted Depth and Actual Depth of Arbitrary Crack 30

List of Figures

Figure 1. FEM Model of Steel Specimen and Crack after Extrude & Subtraction 5
Figure 2. FEM Model with Mesh Control Domains 6
Figure 3. 3D View of Area of Interest 9
Figure 4. 3D (Zoomed In) View of Area of Interest with Mesh Size Locations 9
Figure 5. Mesh Size in Model Builder 10
Figure 6. Mesh Size 1: Boundaries Containing Heat Source and Temperature Probe 10
Figure 7. Mesh Size 2: Sides (Boundaries) of the Crack Within Area of Interest (Zoomed In) 10
Figure 8. Mesh Size 3: Edges of the Crack Within Area of Interest (Zoomed In) 11
Figure 9. Boundaries Removed After Meshing 11
Figure 10. Final Meshing of Entire Domain 12
Figure 11. Final Meshing of Area of Interest (Top View) 12
Figure 12. Number of Elements for the FEM Model with Crack of Depth 1 mm 12
Figure 13. Heat Source Location and Location of T1(c) and T2 (c) 15
Figure 14. The Plot Between Normalized Temperature Index and Depth of The Crack 16
Figure 15. Surface Temperature Contour Plot at 1 Sec 16
Figure 16. Surface Temperature Contour Plot at 2 Sec 17
Figure 17. Surface Temperature Contour Plot at 5 sec 17
Figure 18. Surface Temperature Contour Plot at 5.01 sec 18
Figure 19. Surface Temperature Contour Plot at 5.1 sec 18
Figure 20. Surface Temperature Contour Plot at 5.5 sec 19
Figure 21. Location of Heat Source 20
Figure 22. Time vs (T1-Ti) & (T2-Ti) When Heat Source is at 4 mm from the Crack 21
Figure 23. Time vs (T1-Ti) & (T2-Ti) When Heat Source is at 16 mm from the Crack 21
Figure 24. Time(t) vs Temperature (T1 - Ti & T2 - Ti) for Crack Depth 0.4 mm 23
Figure 25. Time(t) vs Temperature (T1 - Ti & T2 - Ti) for Crack Depth 1.5 mm 24
Figure 26. Time(t') vs Depth of the Crack 25
Figure 27. Best fit curve 26
Figure 28. Time(t) vs Temperature (T1 - Ti & T2 - Ti) for Arbitrary Crack of Depth 0.7 mm 28
Figure 29. Time(t) vs Temperature (T1 - Ti & T2 - Ti) for Arbitrary Crack of Depth 3.8 mm 29
Figure 30. Time(t) vs Temperature (T1 - Ti & T2 - Ti) for Arbitrary Crack of Depth 5.5 mm 29

List of Abbreviations

- *Cp is the specific heat capacity at constant stress (SI unit: J/(Kg.K)*
- *T is the absolute temperature (SI unit: K)*
- *P1 is the temperature probe at (0.25405 mm, 0.25 m, 0.2 m)*
- *P2 is the temperature probe at (0.24085 mm, 0.25 m, 0.2 m) (when laser beam center is at 4 mm from the crack)*
- *T1 is the temperature at P1*
- *T1(c) is the temperature at a point on the heat source side in calibration model*
- *T2(c) is the temperature at a point on the other side of the crack in calibration model*
- *T2 is the temperature at P2*
- *Ti is the initial temperature (293.15 K)*
- *Max.: Maximum*
- *Temp.: Temperature*
- *Diff.:Difference*

Chapter 1: Introduction

Cracks in structures often result in decrease in its strength and may also cause the failure of the structure. Besides loading, the seriousness of the crack depends on the structure's material and the nature of the crack. For example, in steel bridges, the growth of the existing crack may cause the fatigue failure of the structural component or the structure itself with time (Azizinamini et al., 2013). In contrast, in concrete structures, not all cracks represent immediate loss of strength or failure of the structure. Presence of the crack in the concrete structures however, may increase the rate of deterioration because of increase in the water penetration through the crack (Aggelis et al., 2010). The nature of the crack is also important to understand its effect on the structure. If there is crack only in the paint or the plaster then there is no need to repair it. If the crack is penetrating under the surface, then the crack may cause damage to the structure sooner or later. Hence it is important to detect such discontinuities early and repair them (Jung et al., 2018). Nondestructive testing (NDT) techniques can be used for detecting such cracks. In Nondestructive testing (NDT), the part or the assembly of the structure is inspected and tested for discontinuities or differences in characteristics without disturbing its serviceability (*Introduction to Nondestructive Testing*, n.d.). Some of the nondestructive testing techniques are; magnetic particle testing (MT), Liquid Penetrant Testing (PT), Radiographic Testing (RT), Ultrasonic Testing (UT), Electromagnetic Testing (ET), Visual Testing (VT), Laser Testing (LT), Magnetic Flux Leakage (MFL), Thermal/Infrared Testing (IR), Vibration Analysis (VA) (*Introduction to Nondestructive Testing*, n.d.).

The methods specifically used to identify the crack include dye penetrant, magnetic particle inspection, x-ray computer tomography (CT), ultrasound testing (UT) & eddy current testing (ET)(J. Schlichting et al., 2010). These methods have been widely used but have disadvantages as well. Dye penetrant & magnetic particle inspection method are not preferable for determining the crack depth which is perpendicular to the surface and they also require direct access to the surface under investigation. X-ray Computer tomography (CT) method although having great geometrical accuracy is time consuming and expensive. Ultrasound testing gives ambiguous results when testing is done on anisotropic material. Electric current method is limited to electrically conductive materials (J. Schlichting et al., 2010).

Infrared thermography is an alternative to conventional nondestructive inspection methods, which offers a non-contact, wide area detection of subsurface defects. It has many advantages over the other non-destructive methods (Avdelidis et al., 2011). It can be used to investigate a larger area while other techniques are limited to point or line inspection. Furthermore, the results from the infrared thermography are easy to interpret. The infrared thermographic cameras used during the testing are risk free as they don't emit any radiation. They only capture and show the infrared radiation emitted from the material which cannot be seen by naked eye or other regular cameras. However, the infrared thermography also comes with some limitation.

One disadvantage of infrared thermography is that it may get influenced by environmental conditions while performing the test outdoor (Avdelidis et al., 2011). Despite some disadvantages, infrared thermography is increasingly used in a number of NDT problems in production and maintenance (J. Schlichting et al., 2010).

There are two approaches in Infrared Thermography; passive approach and active approach. The passive approach tests structures which are naturally at different (often higher) temperature than the ambient temperature. While in active approach an external source (i.e. heat lamps, flash lamps etc.) is required to create a relevant temperature difference. One of the various approaches used in active thermography is pulsed heating transient thermography. In this technique, the specimen is heated for a short period of time and then the temperature decay curve is recorded. Even in pulse thermography various configurations are possible for example; point inspection, line inspection & surface inspection. In point inspection, point heating source (e.g. laser or focused light beam) is used as the source stimuli. In line inspection line lamps, heating wire, scanning laser and line of air jets could be used as external heating source. In surface inspection, heating is done by lamps or scanning laser (Maldague, 2002).

Many works have been done in past for detecting the crack by using laser thermography. In a research done by Rashed et al. in 2007, the location of fatigue crack was determined by heating the surface with the point laser and analyzing the shape of the laser spot image. Two heating methods were used, and the results were compared. First, long pulse heating was done by an argon ion laser and then pulsed laser heating was used for laser spot heating. Thermographic images were then captured with the laser beam at various distances from the fatigue cracks by means of a cedip infrared camera. The heat flow being disturbed by the presence of the crack can be seen in the infrared images and hence depicting the location and the size of the crack. This method however cannot be applied to the cracks perpendicular to the surface. Another limitation of this method is that the heat flow disturbance is visible only when the laser incident point is within 4 mm from the cracks (Rashed et al., 2007).

Similar work was performed by Li et al (2010). The article presents a second derivative image processing technique to form a direct image of the crack. The modelling result from the article determined that the thermal images are affected by laser power, pulse duration, material, crack geometry, image observation time and spot distance from the crack. The optimum imaging distance of the laser spot center from the crack was found to be equal to one radius of the spot size. The paper also studied about the variation of the temperature difference across a crack with respect to different crack openings, change in crack length and different crack depth (Li et al., 2010). The results helped in understanding the limitation of the laser spot imaging. However, the laser heating was applied for less than a second and the laser beam's capacity was just 21 watts (Li et al., 2010). In 2011, Li et al. proposed using laser line instead of laser spot for crack imaging which was faster in comparison to spot thermography for depicting the location of the crack.

Another promising work on detecting the surface breaking cracks was done by Burrows et al.(2011). The research was based on using a laser source to deposit heat into a sample surface. Any defect would block the heat flow. The change in temperature profile caused can then be detected using a thermal imaging camera. Similarly, Schlichting et al.(2012) used spot thermography technique in which surface cracks were detected with the help of a continuously scanning laser together with a fixed infrared camera. No information about the laser spot position or the scanning speed were needed for extracting the image. Additionally, there was no need of synchronization between laser and camera. The results were promising and were also checked with the results from magnetic particle testing (Schlichting et al., 2012).

Most of the articles described above were more emphasized on the crack location and position rather than the crack's penetration depth perpendicular to the surface. J. Schlichting et al.'s work published in 2010 has more insight in to the crack depth determination. For that they used the active thermography and performed an advanced quantitative analysis. The analysis used the difference between the measured transient intensities of thermal radiation in two reference areas equidistant from the laser-spot for determining crack depth. The integration of the expression consisting the difference in intensities over time was defined as crack depth. The analysis however had high signal to noise ratio (Schlichting et al., 2010). Additionally, although the results of the work were robust, further simulations and experiments are needed to understand the effects of depth and gap in temperature differentials (Schlichting et al., 2010).

With the help of infrared thermography, a graphical relation between the temperature index and various crack depths is shown in an article by Basheer et al. (2015). In their work, temperature at two points were measured. One being in the laser spots side and other in the opposite side of the crack. Then the temperature difference between these two points were used to determine the temperature index. The experimental results of temperature index for crack depths of 0.25 mm to 5 mm were compared with the 3D finite element simulation modelled using COMSOL Multiphysics. The results were close enough with average error ranging from 1.113% to 4.01%. In the article, the temperature index for depths of 2 mm - 5 mm is exactly the same in finite element modelling results and is differing by up to 0.003 in experimental results (Basheer et al., 2015). Hence, although the article establishes a graphical relationship between the crack depth and the temperature index, it is hard to predict the depth of an arbitrary crack of depths higher than 2 mm by using this graphical relationship.

In this article, the graphical relationship of the depth of crack with the maximum temperature differential between the points on each side of the crack is presented. Unlike J. Schlichting et al.(2010), the research purposes a simpler approach in which the relationship between the crack depth and temperature differential ratio is obtained by using polynomial regression. The laser of higher power (100 w) and duration (< 5 sec) was used. The boundary conditions of the test specimen are applied such that they don't affect the conduction of the heat from the laser spot to the other side of the crack. Crack length is made long enough so that the heat won't propagate from the sides of the crack. The width of the crack is kept constant so that the depth is the only variable. The position of the heat source and the two temperature probes is same in all the data collections. A brief explanation of heat source's location is described in results section.

Chapter 2: Finite Element Modelling

COMSOL Multiphysics 5.5 is used to model the Steel Specimen (0.5 m x 0.5 m x 0.2 m) with cracks of 0.5 m long x 0.1 mm wide x (0.1 mm – 7 mm) deep. The modelling is subdivided in to following sections.

Geometry:

First, two-dimensional geometries were created using square of size 0.5 m x 0.5 m for the steel specimen and rectangle of size 0.5 m x 0.1 mm for the crack. Then the extrude command was used to convert them into three dimensional objects. Finally, both the extrudes were subtracted using Boolean and Partition to create the crack.

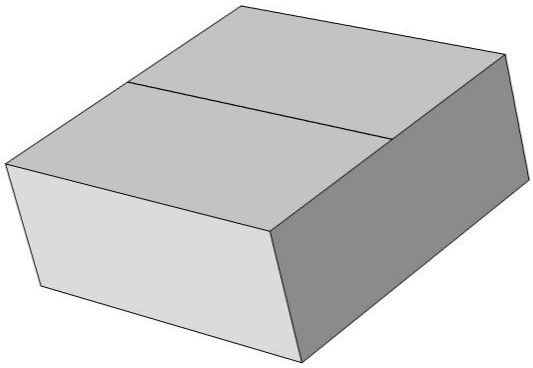

Figure 1. FEM Model of Steel Specimen and Crack after Extrude & Subtraction

While creating the geometry, for efficient meshing, the domain is divided into multiple domain using Partition Domain as shown in Table 1 and Figure 2. Using Mesh Control Domain(Frei, 2015a), all these domains would be removed after meshing. which is discussed in detail in meshing sub section.

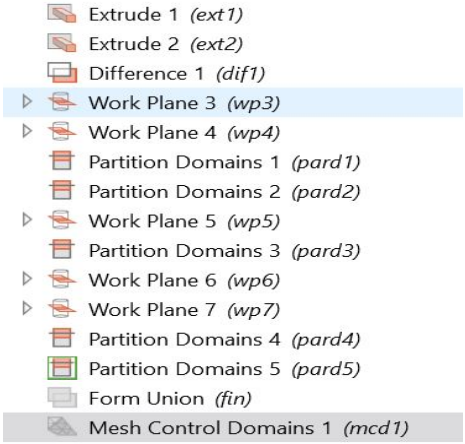

Table.1. Partition Domain & Mesh Control Domain

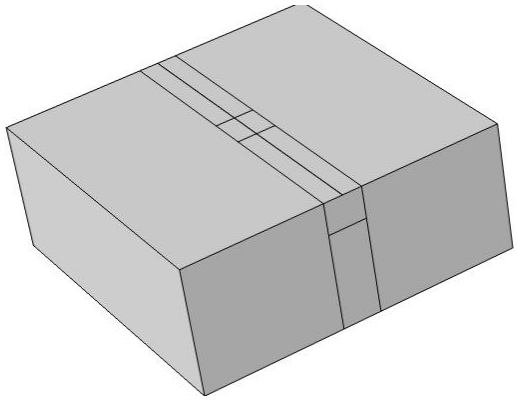

Figure 2. FEM Model with Mesh Control Domains

Material Properties:

Inbuild structural steel was used as the specimen material. The basic properties are shown below. The emissivity of the material is taken as 0.79.

Name	Value	Unit
Heat capacity at constant pressure	475[J/(kg*K)]	J/(kg·K)
Thermal conductivity	44.5[W/(m*K)]	W/(m·K)
Density	7850[kg/m^3]	kg/m³

Table.2. Test Specimen and Crack after Extrude & Subtraction

Heat Source and Heat Transfer in Solids:

Heat Source

The radius and the power of the Laser Beam used are 2 mm and 100 watts respectively which is defined under Parameter 1 shown in Table 3. The effect of laser beam was modelled by means of heat flux which is equal to the emissivity of the material times the laser heat flux. This is presented in Table 4.

Name	Expression	Value	Description
r_spot	2 [mm]	0.002 m	Laser Radius
emissivity	0.79	0.79	Emissivity of the Material
p_laser	100 [W]	100 W	Laser Power

Table.3. Parameter 1

Name	Expression	Unit	Description
x_focus	0.24595 [m]	m	x location of laser focal point
y_focus	0.25[m]	m	y location of laser focal point
r_focus	sqrt((x - x_focus)^2 + (y - y_focus)^2)	m	distance from the focal point
flux	((2*p_laser/(pi*r_spot^2))*exp(-(2*r_focus^2)/r_spot^2))*(t<5)	W/m²	Laser heat flux, Gaussian profile

Table.4. Variables 1

The laser heat flux is assumed to have gaussian profile of equation shown in above table (*Laser Heating of a Silicon Wafer*, n.d.)(Frei, 2015b). The location of the laser incident point is fixed which is indicated by x_focus and y_focus in Table 4. This is explained in detail in results section.

Heat Transfer in Solids

It has been found that for a solid specimen the difference between 3D temperature distribution with and without considering the radiation was less than 10^{-4} K (J. Schlichting et al., 2010). So, the influence of heat transfer caused by radiation in such case is negligible in comparison to conduction (J. Schlichting et al., 2010). Hence, in this thesis only the heat transfer in solids due to conduction is modelled. The equation for heat transfer through conduction is (COMSOL Multiphysics, 2015),

$$\rho C_p \frac{\partial T}{\partial t} + \rho C_p \mathbf{u} \cdot \nabla T + \nabla \cdot \mathbf{q} = Q + Q_{\text{ted}}$$

$$\mathbf{q} = -k \nabla T$$

Where,

- Cp is the specific heat capacity at constant stress (SI unit: J/(kg·K))
- T is the absolute temperature (SI unit: K)

- **u** is the velocity vector of translational motion (SI unit: m/s)
- **q** is the heat flux by conduction (SI unit: W/m2)
- α is the coefficient of thermal expansion (SI unit: 1/K)
- Q=0; contains additional heat sources (SI unit: W/m3)
- k is thermal conductivity (SI unit: W/(m·K))
- Q_{ted} =0; is the thermoelastic damping and account for the thermoelastic effects in solid.

For discretization in 'Heat Transfer in Solids' in COMSOL, the default element used is Quadratic Lagrange. The initial value for the temperature is 293.15[k]. Thermal insulation is used as boundary condition. As mentioned earlier the heat flux absorbed by the material called inward heat flux in the COMSOL is equal to emissivity x flux.

Mesh

Meshing of the model is done in various steps. Since this is a 3D finite element model with depth of the crack being very small (0.1 mm to 7 mm), small change in element size may vary our result. Hence, finer mesh is used around the area of interest and coarser mesh is used at locations away from the area of interest. The area of interest shown in figure 3 & 4 is the area that includes the vicinity of the heat source & the probe at the other side of the crack at which we are measuring the temperature.

As mentioned in geometry section (Figure 2), the domain is subdivided into multiple sub domain so that we can mesh individual domains separately.

The elements used are either free tetrahedral or triangular. The maximum and minimum element size is user controlled. All together six sizes are used for meshing as shown in Figure 5. First, a coarser meshing of entire domain is done with element size ranging from 0.25 m to 1.0 E-3 m. Then in Size 1, the boundaries containing the laser center and the probe are meshed with finer elements of size 0.001 m to 1.0 E-5 mm as shown in Figure 6. Because of comparatively minute element size, the boundaries and edges of the crack in the area of interest are then meshed with even more fine element size. In Size 2, a finer meshing of element size 0.001 m to 1.0 E -5 m is applied on boundaries 22,24 & 26 as shown in Figure 7. In Size 3, the same meshing size as of Size 2 is applied to edges of the crack around the area of interest (Figure 8). Size 4 and Size 5 are also edge meshing of the edges which were away from the area of interest.

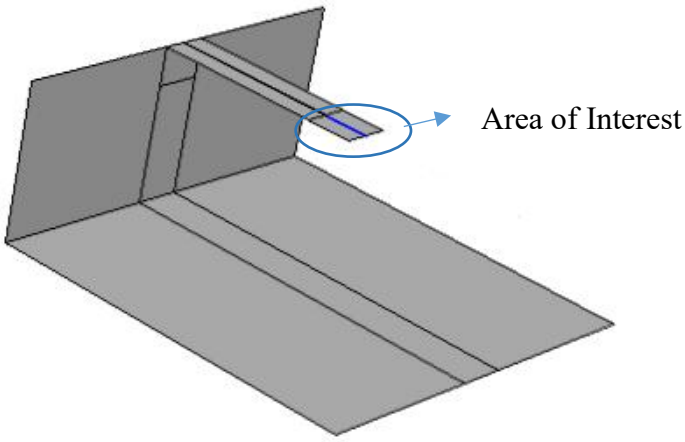

Figure 3. 3D View of Area of Interest

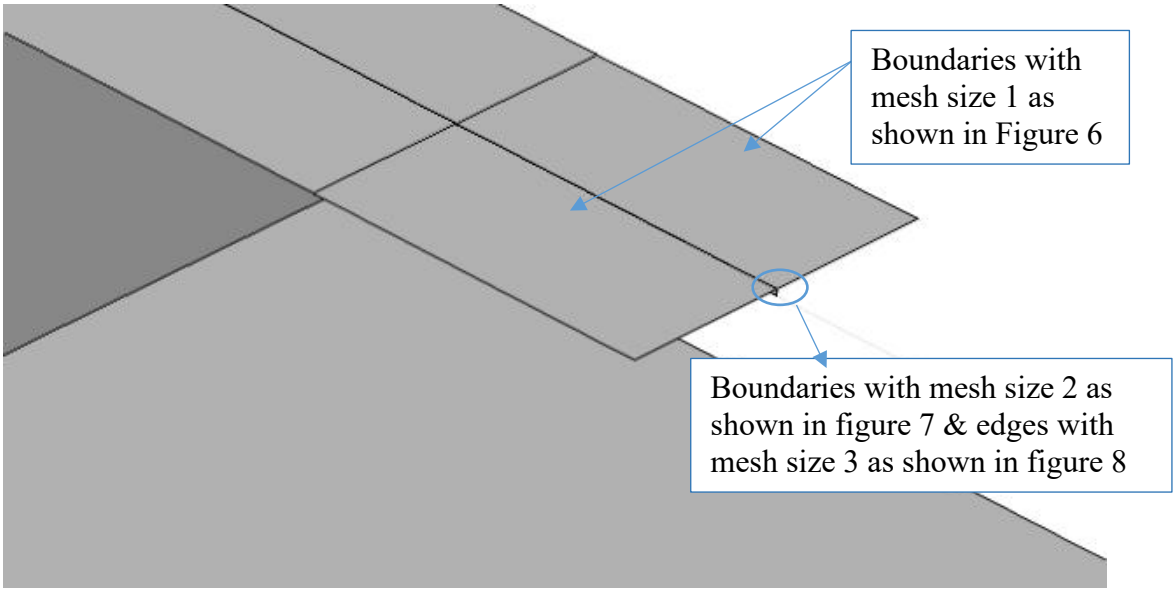

Figure 4. 3D (Zoomed In) View of Area of Interest with Mesh Size Locations

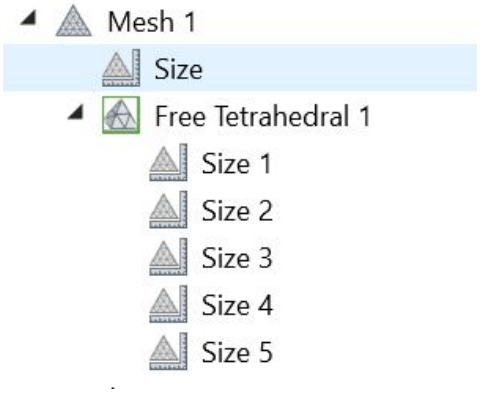

Figure 5. Mesh Size in Model Builder

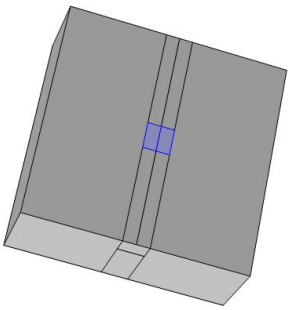

Figure 6. Mesh Size 1: Boundaries Containing Heat Source and Temperature Probe

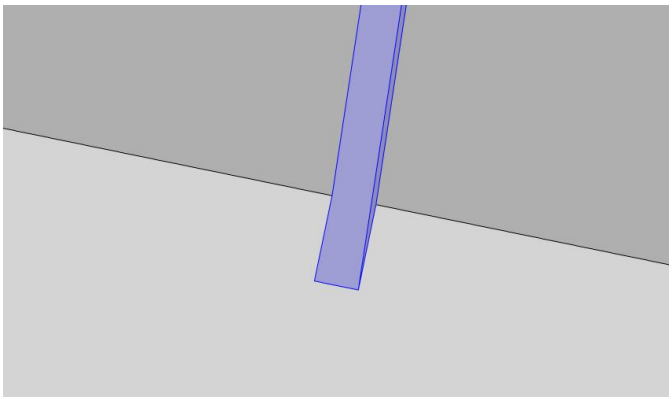

Figure 7. Mesh Size 2: Sides (Boundaries) of the Crack Within Area of Interest (Zoomed In)

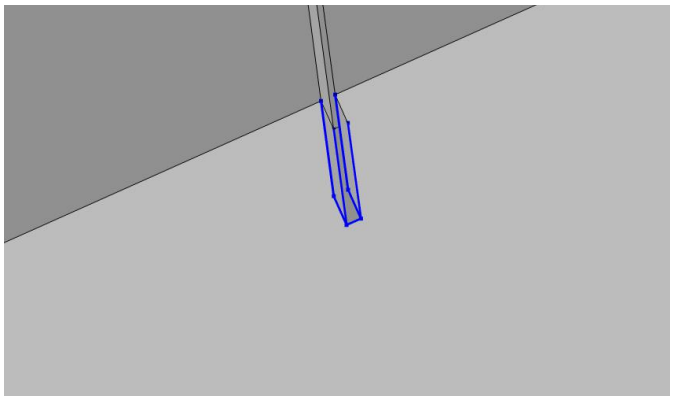

Figure 8. Mesh Size 3: Edges of the Crack Within Area of Interest (Zoomed In)

It should be noted that because we are using Mesh Control Domain (Frei, 2015a), all the boundaries and partition domains that were created just for meshing gets removed after mesh completion. A screen shot of Settings of Size 2 Mesh is shown in Figure 9. It can be seen that the boundaries are removed after meshing. The final mesh of the entire domain is shown in Figure 10 and that of the area of interest is shown in Figure 11.

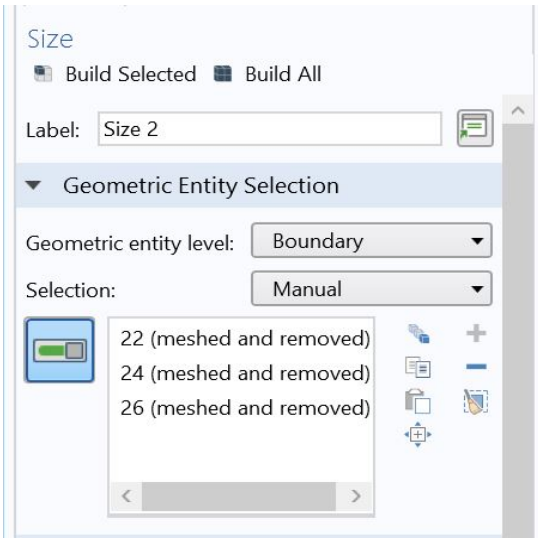

Figure 9. Boundaries Removed After Meshing

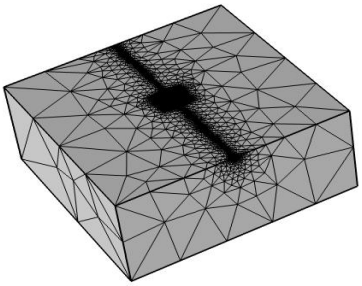

Figure 10. Final Meshing of Entire Domain

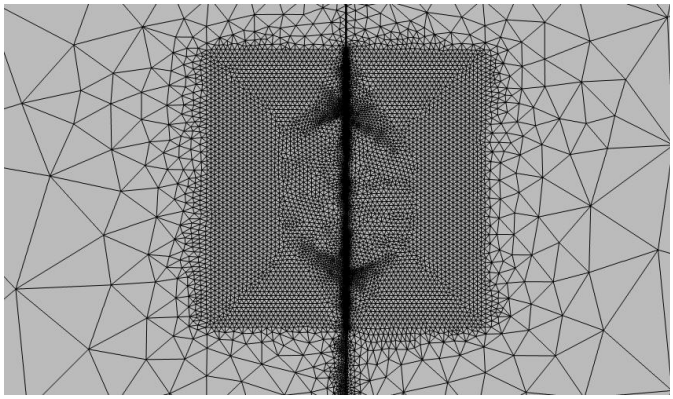

Figure 11. Final Meshing of Area of Interest (Top View)

The advantage of using Mesh Control Domain is that we need not to assign material properties to every domain. A table for total number of mesh for a crack of depth 1 mm is shown below. It should be noted that the model has large number of elements and took from 20-40 minutes to run one analysis.

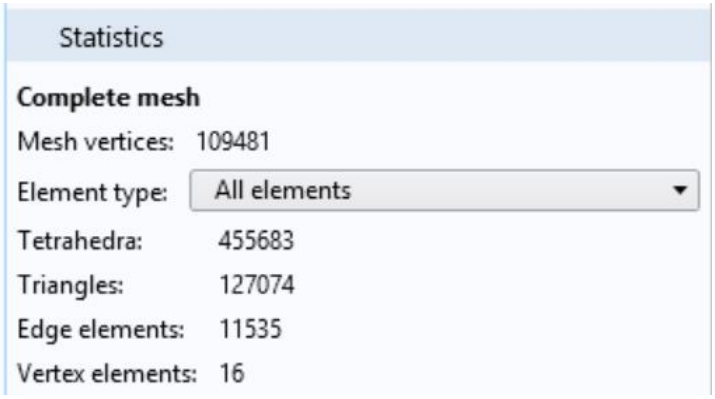

Figure 12. Number of Elements for the FEM Model with Crack of Depth 1 mm

Study Settings

A time dependent study was conducted within a range of 0 to 10 seconds and the data was collected with the time step of 0.01 sec. Both the relative and absolute tolerance were set to be 0.0001 for accuracy.

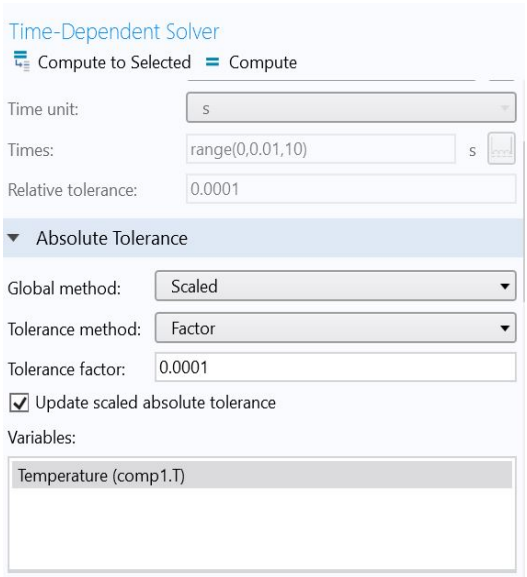

Table.5. Time Dependent Solver Settings

The Implicit Backward Differentiation Formula was used by the software for the computation with the initial step of 0.001 sec. Further information can be seen in the Table below.

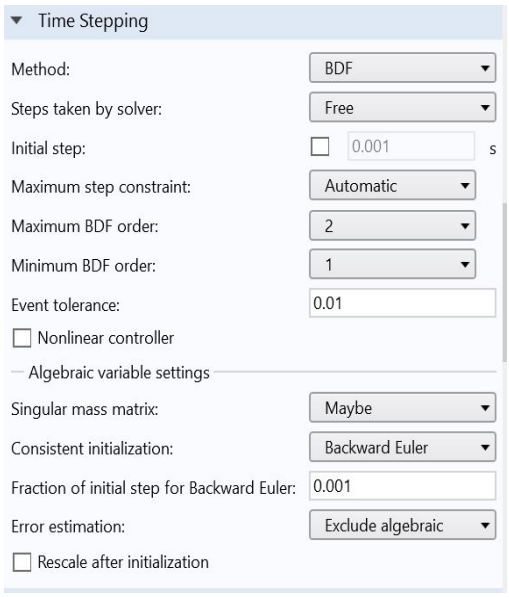

Table.6. Time Stepping Settings

Model Calibration

For the calibration of the finite element model, the results from the model were compared with the experimental results from Basheer et al., 2015. The width of the crack, laser properties, location of the center of the laser beam and the scale used for normalizing the temperature differential were different in the experiment performed by Basheer et al. (2015). Accordingly, for calibration, the crack width was changed to 1 mm. An approximate modelling of the heat source with laser power 2W and pulse duration 3.76 ns is done. The location of the heat source is also approximated in a way similar to left side heating experiment done by Basheer et al. (2015) as shown in figure 13. T1(c) and T2(c) are the temperatures at two points equidistance from the crack. T1(c) is on the heat source side and T2(c) is on the other side of the crack. For normalizing the temperature difference, an average of ambient temperature which is 293.15 K in our case was used at the denominator. The scale factor used is 1000.

The base line for the modelling calibration was the crack of depth 0.5 mm. Then the same settings were used for the different depths. Finally, the normalized temperature index were calculated for each depth as shown in table below. The results were promising with error range of 5.29% to -5.96%. A graphical representation has also been established as shown in figure 14.

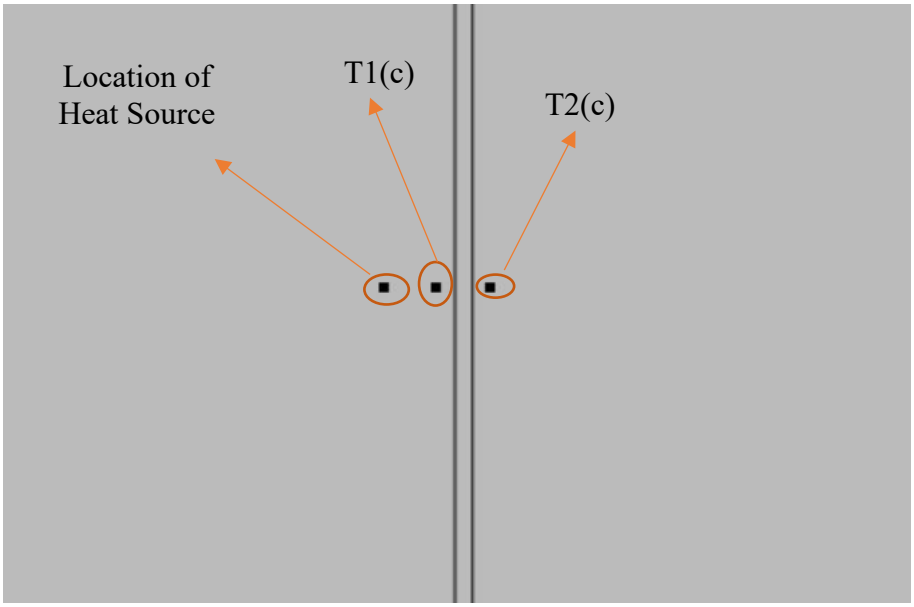

Figure 13. Heat Source Location and Location of T1(c) and T2 (c)

Depth(mm)	Experimental Result (Basheer et al., 2015)	Results from Simulation	Error(%)
0.25	1.996	2.115	-5.96
0.5	2.408	2.354	2.24
1	2.665	2.524	5.29
1.5	2.7	2.593	3.96
2	2.71	2.763	-1.96
2.5	2.712	2.831	-4.39
3	2.706	2.831	-4.62
3.5	2.708	2.831	-4.54
4	2.7087	2.831	-4.52
5	2.71	2.831	-4.46

Table.7. Comparison between Experimental and Simulation Results

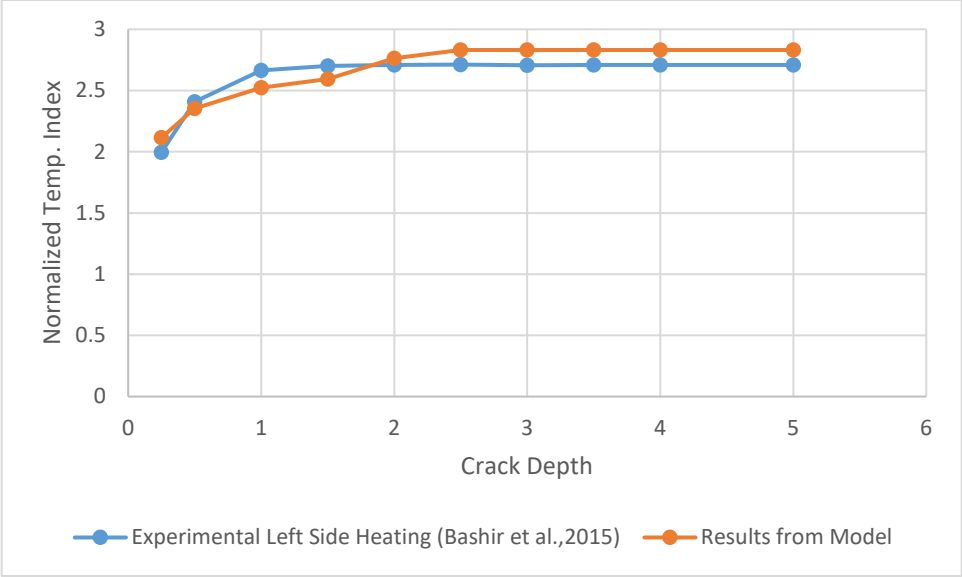

Figure 14. The Plot Between Normalized Temperature Index and Depth of The Crack

Results from Finite Element Analysis

FEM analysis with cracks of fifty different depths were performed. Some of the zoomed in plots of the surface temperature contour for a crack of depth 1 mm at various time steps are shown below.

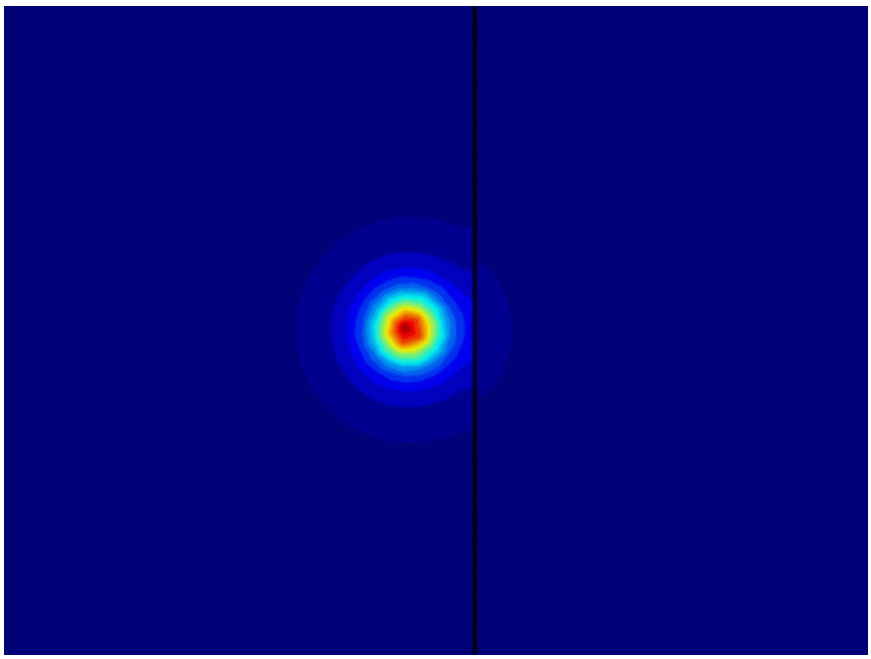

Figure 15. Surface Temperature Contour Plot at 1 Sec

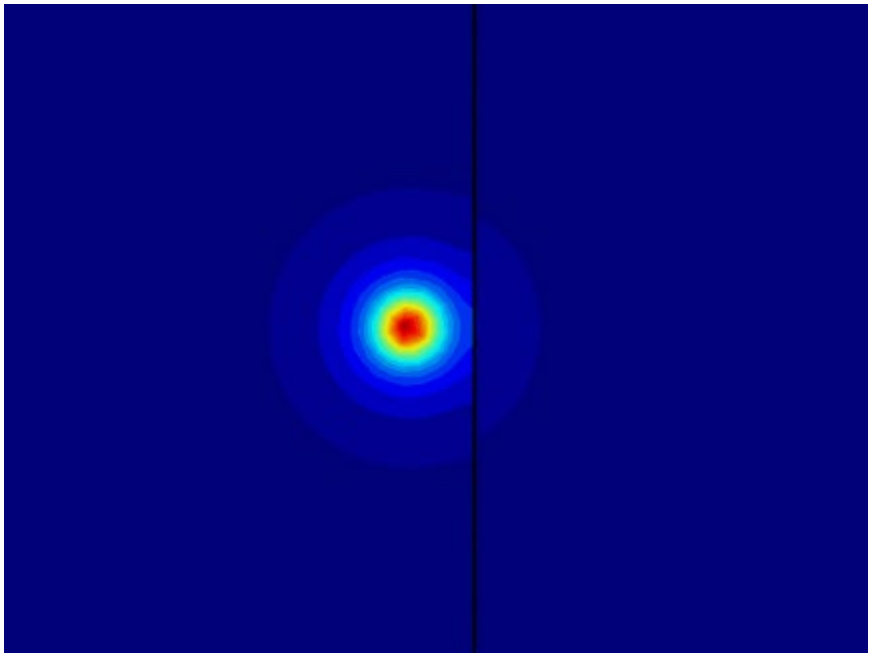

Figure 16. Surface Temperature Contour Plot at 2 Sec

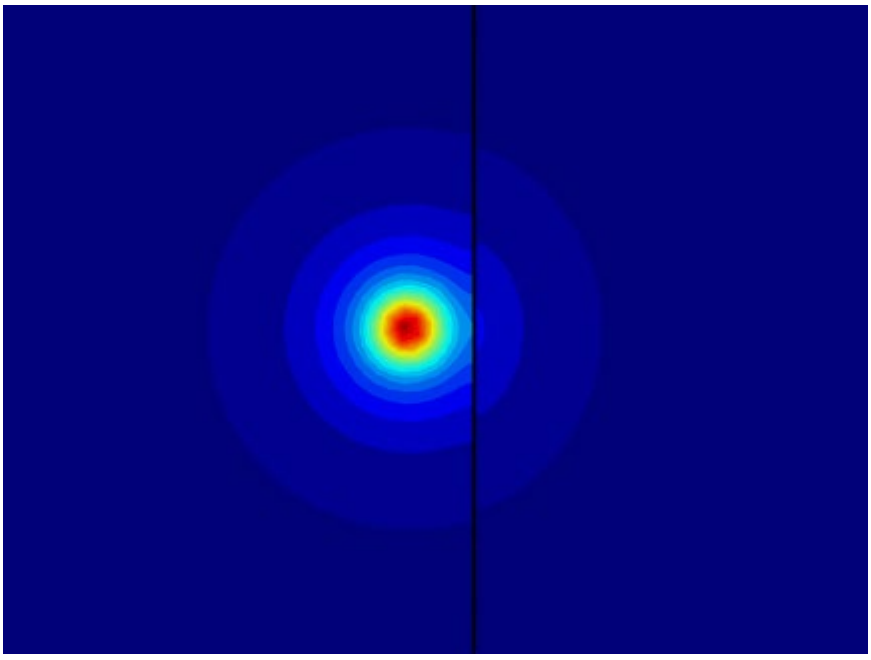

Figure 17. Surface Temperature Contour Plot at 5 sec

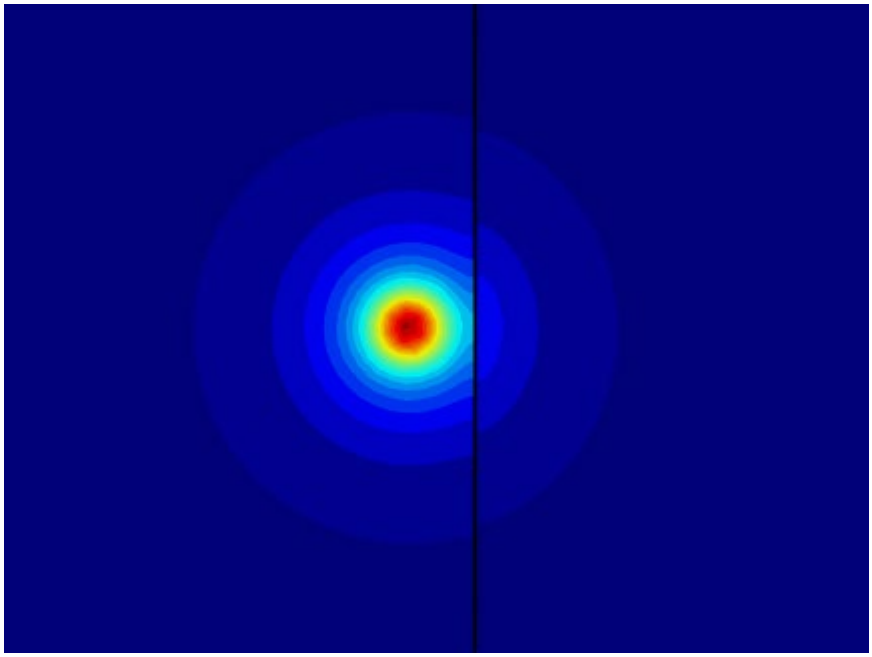

Figure 18. Surface Temperature Contour Plot at 5.01 sec

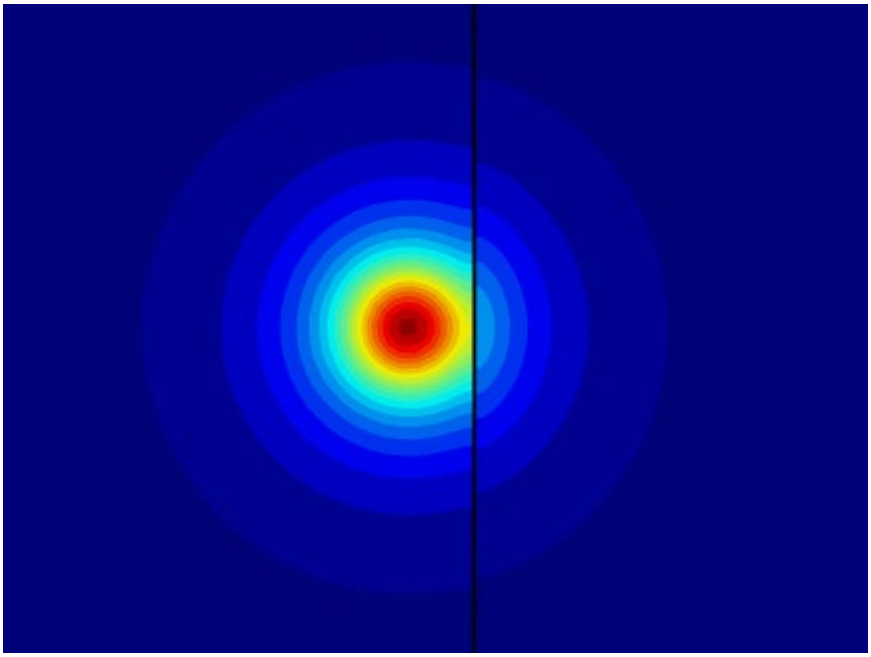

Figure 19. Surface Temperature Contour Plot at 5.1 sec

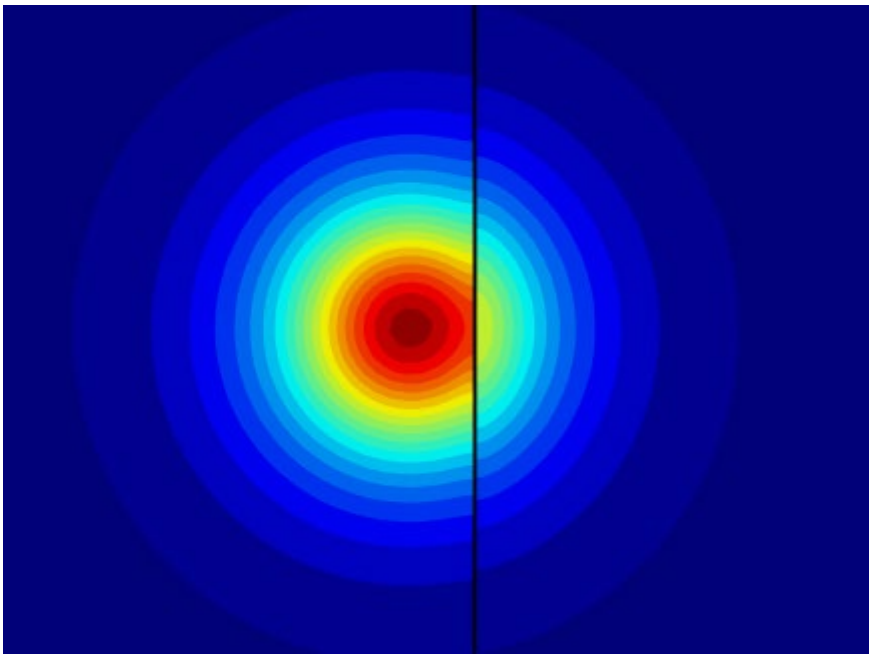

Figure 20. Surface Temperature Contour Plot at 5.5 sec

Two of the point domain probes (P1 and P2) were created on both sides of the heat source and temperature at those probes were determined by the FEM Analysis. Probe P1 was at right side of heat source (beyond crack) and P2 was at left side of the heat source (in non-damaged side). Both of them were at same distance from the center of the heat source. The temperature profile for the probe P2 (in non-damaged side) will not change because of the change in depth of the crack. Hence, to save time required to run each analysis, single Probe P2 data was used for all of the cases. Beyond data from P2; P1 alone will have 1000 temperatures for each depth at a time increment of 0.01 sec from 0 to 10 seconds. Hence for 50 cases, total data for P1 will be around 50000. Because of the bulk amount of data, only the plot between the time and temperature difference for each crack has been attached in Appendix A.

To figure out the possible locations of the heat source, two different finite element modelling were studied by moving the location of the laser incident away from the source. The 'optimum' imaging distance of the laser spot center from the crack is found to be equal to one radius of the spot size (Li et al., 2010). In our case it is supposed to be 2 mm from the crack since the radius of our laser beam is 2 mm. However, the source couldn't be located at 2 mm or 3 mm from the crack because of the modelling complication. The first guessed location is at 4 mm from the crack. To see the temperature variation, second location is kept at 16 mm from the crack. The model with the heat source at 16 mm was plotted with a time step of 0.1 mm due to resource limitations. The temperature data at probes P1 and P2 were taken for both the cases. It should be noted that the distance of laser beam center from both P1 and P2 is equal. Since, the Probe P1 is fixed but the source is moving, the position of probe P2 changes accordingly. The modelling was done for only one depth (1 mm).

Then the temperature differential between source P1 and P2 for both locations of the heat source (laser beam) was noted and plotted as shown in figure 22 and figure 23.

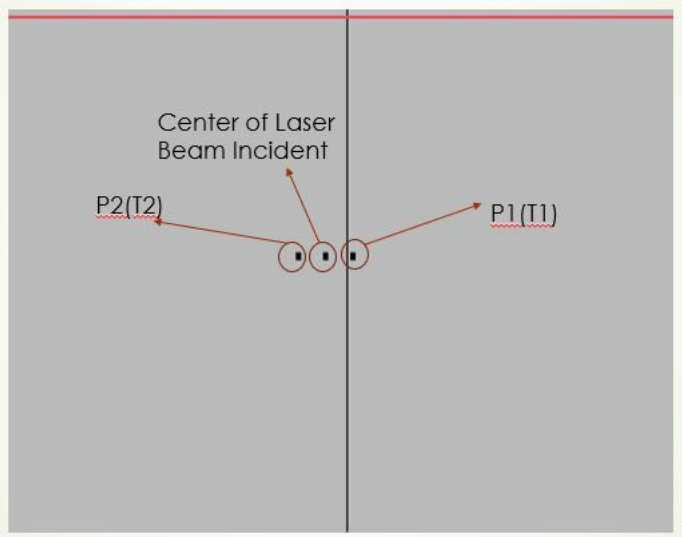

Figure 21. Location of Heat Source

Name	Expression	Unit	Description
x_focus	0.24595 [m]	m	x location of laser focal point
y_focus	0.25[m]	m	y location of laser focal point

Table.8. Location of Heat Source at 4 mm from the Crack

Name	Expression	Unit	Description
x_focus	0.23395 [m]	m	x location of laser focal point
y_focus	0.25 [m]	m	y location of laser focal point

Table.9. Location of Heat Source 16 mm from the Crack

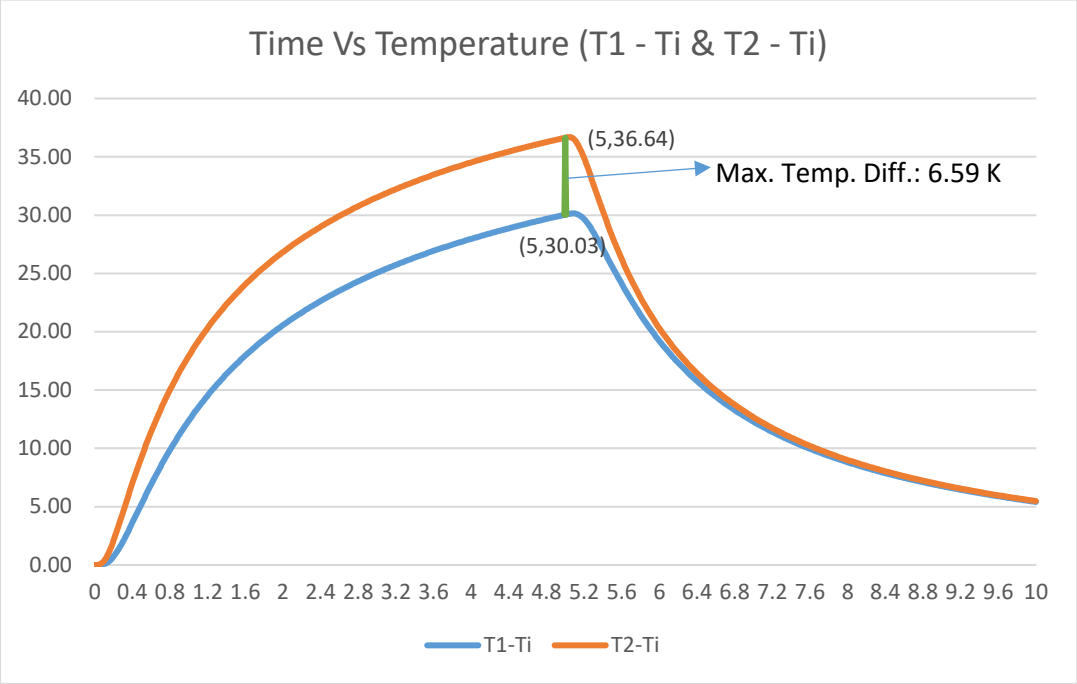

Figure 22. Time vs (T1-Ti) & (T2-Ti) When Heat Source is at 4 mm from the Crack

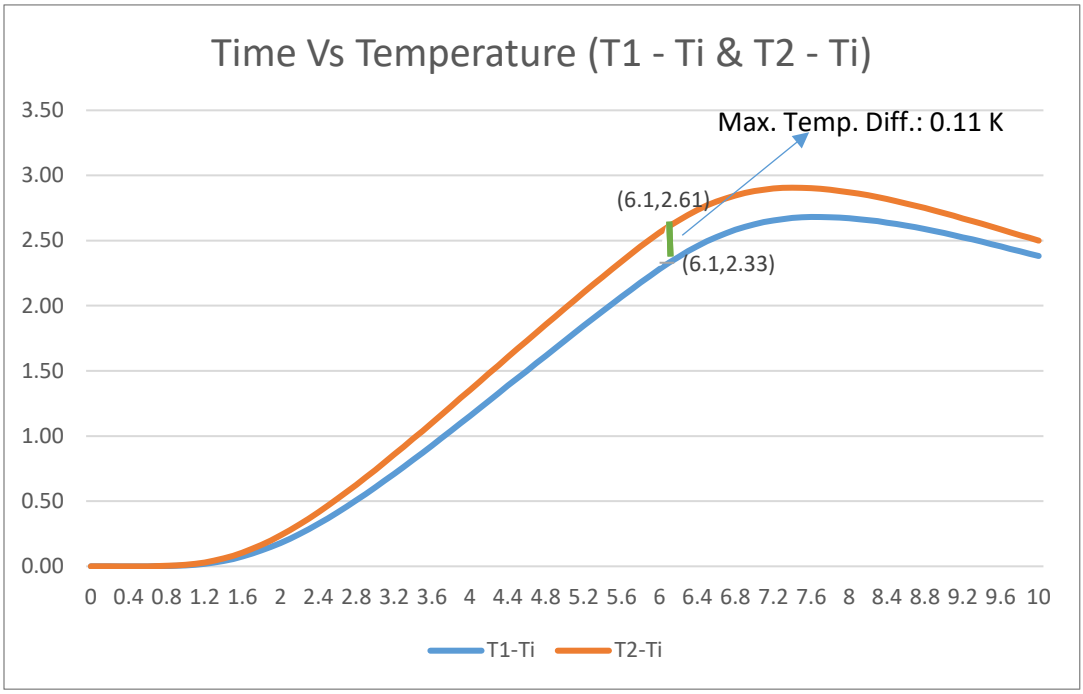

Figure 23. Time vs (T1-Ti) & (T2-Ti) When Heat Source is at 16 mm from the Crack

It can be inferred from the plots that the temperature differential between two curves (T1-Ti) & (T2-Ti) is more evident (6.59 K) when the laser beam incident point is at 4 mm from the crack. Additionally, the time (5.0 sec) to reach the maximum differential is less in case of heat source at 4 mm from the crack than heat source at 16 mm from the crack for the same crack depth (1 mm). Hence, for this thesis the center of the laser beam is located at 4 mm from the crack.

Chapter 3: Data Analysis

Data Collection from FEM Analysis

Temperature at probes P1 and P2 were exported for each crack from FEM Analysis results. Ti is the initial temperature (293.15 K) which is subtracted from the temperatures at both the probes. Time vs Temperature plot for the crack of depth 0.4 mm and 1.5 mm is shown in figure 16 & 17. Where T1 is the temperature at P1 and T2 is the temperature at P2 at time interval of 0.01 second from 0 to 10 seconds respectively. The plot for all of the cracks is shown in Appendix A.

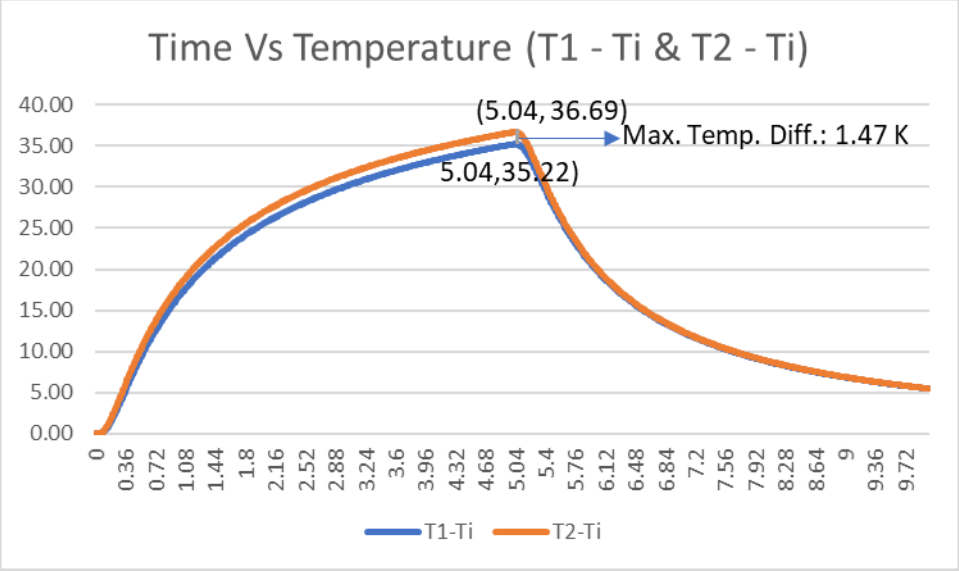

Figure 24. Time(t) vs Temperature (T1 - Ti & T2 - Ti) for Crack Depth 0.4 mm

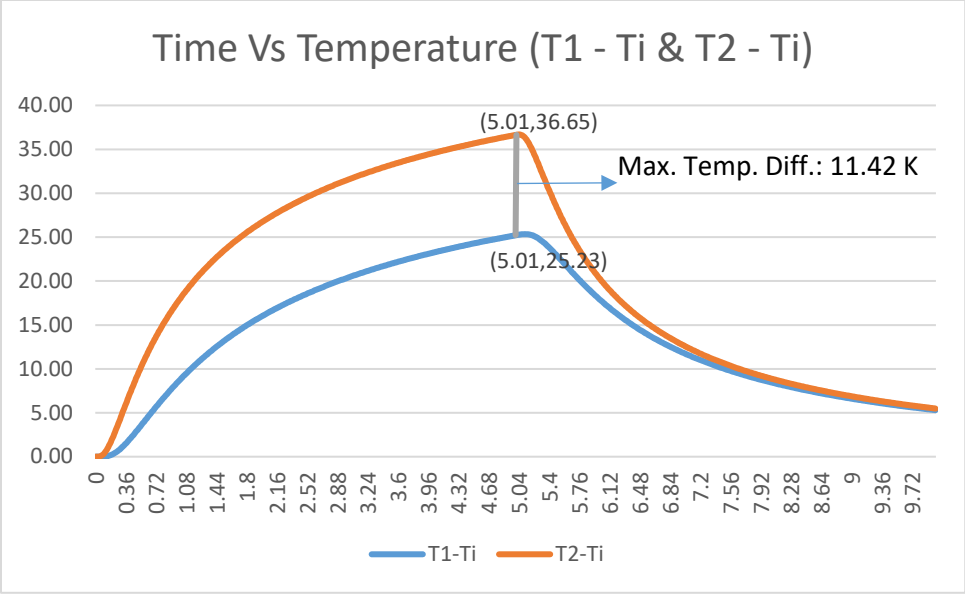

Figure 25. Time(t) vs Temperature (T1 - Ti & T2 - Ti) for Crack Depth 1.5 mm

By using the data from FEM analysis, a difference of (T1 – Ti) and (T2 – Ti) was also calculated. Then the Excel Max Function was used to calculate maximum of (T1 – Ti) – (T2 – Ti) was obtained, which is same as the maximum difference seen in the curve above. Next, Excel's Index and Match function were used to get the time (t') at which the maximum difference occurred is also obtained. Value of (T2 – Ti) is then noted at time t'. Finally, the ratio of ((T1 – Ti) – (T2 – Ti))/ (T2 – Ti) @t' is calculated. This procedure is repeated for each depth. Hence, for 50 different depths, we will have 50 different values of (T1 – Ti) – (T2 – Ti)/ ((T2 – Ti) @t' as shown in Table 11.

A table showing the time (t') at which the maximum temperature difference occurs, and the corresponding depth of the crack is shown in Table 10. The corresponding plot is also shown in Figure 18.

Depth (mm)	Time (sec) at Max. Temp. Diff
0.1	5.07
0.2	4.01
0.3	3.46
0.4	5.04
0.5-0.9	5
1.1-1.9	5.01
2.0-4.0	5.02
4.1-6.5	5.03

Table.10. Time(t') & Depth of the Crack

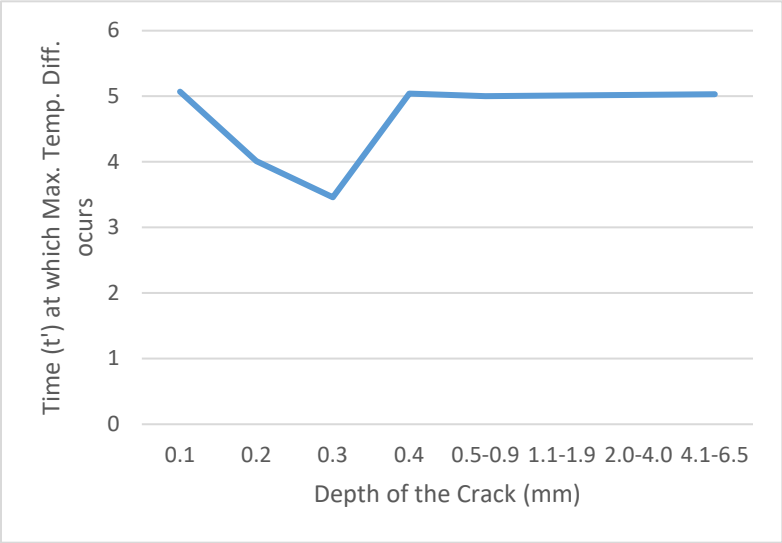

Figure 26. Time(t') vs Depth of the Crack

It can be seen from the table and the graph that the maximum time required to achieve the maximum temperature difference is 5.07 sec (for 0.1 sec). Which is just 0.07 sec beyond the time at which the source is turned off. For cracks of depth beyond 0.5 mm, there is minor increase in time (t').

Regression Analysis

As mentioned earlier, polynomial regression analysis was performed with depth of the crack as the dependent variable and the index ((T1 – Ti) – (T2 – Ti))/ ((T2 – Ti) @t' as the independent variable. The data used is shown in Table 11. The regression was done in MATLAB using Polyfit function. The coding is shown in Appendix B.

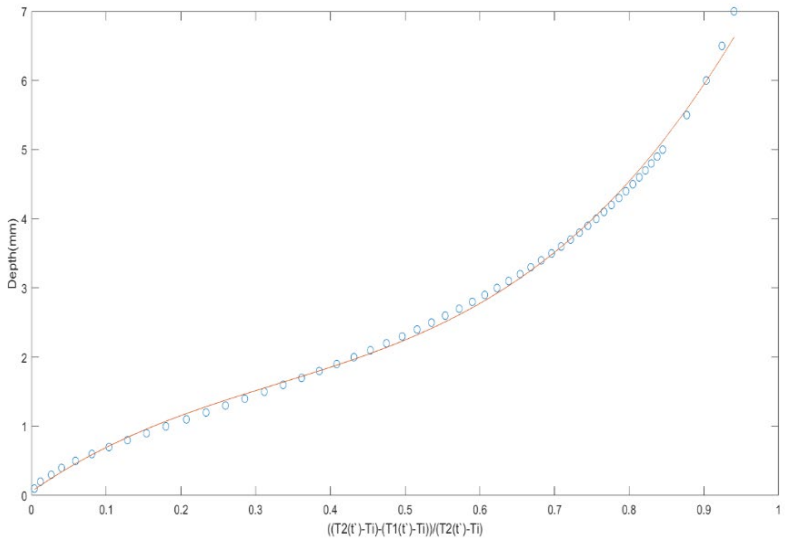

Figure 27. Best fit curve

The equation obtained for depth of the crack is

$y = 12.9873x^3 - 12.7914x^2 + 7.5291x + 0.058$; with $R^2 = 0.9974$----------(iii)

where,

x = Temperature differential index = ((T2(t')-Ti)-(T1(t')-Ti))/(T2(t')-Ti)

y = Predicted Depth of the Crack

X= ((T2(t')-Ti)-(T1(t')-Ti))/(T2(t')-Ti)=	Depth(mm)	Predicted Depth (y)(mm)	Error (mm)	Error %
0.0039	0.1	0.1	0.0	0.00
0.0119	0.2	0.2	0.0	0.00
0.0263	0.3	0.3	0.0	0.00
0.0401	0.4	0.4	0.0	0.00
0.0589	0.5	0.5	0.0	0.00
0.0808	0.6	0.6	0.0	0.00
0.1285	0.8	0.9	-0.1	12.50
0.1540	0.9	1.0	-0.1	11.11
0.1799	1	1.1	-0.1	10.00
0.2074	1.1	1.2	-0.1	9.09
0.2337	1.2	1.3	-0.1	8.33
0.2597	1.3	1.4	-0.1	7.69

0.2855	1.4	1.5	-0.1	7.14
0.3117	1.5	1.6	-0.1	6.67
0.3368	1.6	1.7	-0.1	6.25
0.3614	1.7	1.8	-0.1	5.88
0.3852	1.8	1.9	-0.1	5.56
0.4085	1.9	1.9	0.0	0.00
0.4315	2	2.0	0.0	0.00
0.4536	2.1	2.1	0.0	0.00
0.4751	2.2	2.2	0.0	0.00
0.4961	2.3	2.3	0.0	0.00
0.5161	2.4	2.4	0.0	0.00
0.5353	2.5	2.5	0.0	0.00
0.5538	2.6	2.6	0.0	0.00
0.5725	2.7	2.7	0.0	0.00
0.5900	2.8	2.8	0.0	0.00
0.6067	2.9	2.9	0.0	0.00
0.6229	3	3.0	0.0	0.00
0.6387	3.1	3.1	0.0	0.00
0.6540	3.2	3.2	0.0	0.00
0.6682	3.3	3.3	0.0	0.00
0.6822	3.4	3.4	0.0	0.00
0.6960	3.5	3.5	0.0	0.00
0.7088	3.6	3.6	0.0	0.00
0.7214	3.7	3.8	-0.1	2.70
0.7448	3.9	4.0	-0.1	2.56
0.7560	4	4.1	-0.1	2.50
0.7662	4.1	4.2	-0.1	2.44
0.7763	4.2	4.3	-0.1	2.38
0.7863	4.3	4.4	-0.1	2.33
0.7956	4.4	4.5	-0.1	2.27
0.8048	4.5	4.7	-0.2	4.44
0.8133	4.6	4.8	-0.2	4.35
0.8217	4.7	4.9	-0.2	4.26
0.8297	4.8	5.0	-0.2	4.17
0.8374	4.9	5.1	-0.2	4.08
0.8448	5	5.2	-0.2	4.00
0.9032	6	6.0	0.0	0.00
0.9240	6.5	6.4	0.1	1.54
0.9403	7	6.7	0.3	4.29

Table.11. Temperature Differential Index and Crack Depth (Actual depth used for regression & depth from the regression equation)

Chapter 4: Checking the Result for a Crack of Arbitrary Depth

The purpose of the finite element modelling and regression analysis in this thesis is to present a framework by which depth of any crack visible on the surface can be depicted. In this chapter, the process is described and is applied to three arbitrary cracks. Since, experimental data is not available, the temperature index is obtained by finite element modelling.

Three cracks of depths 0.7 mm, 3.8 mm and 5.5 mm were modelled in COMSOL and analyzed to get the temperature index. The size of the steel specimen was 0.5 m x 0.5 m x 0.2 m. The plan of the crack was of dimension 0.5 m x 0.1 mm. The Extrude, Boolean and Partition commands were used to create the crack and three-dimensional model. Then the heat source is modelled as heat flux from a laser beam of radius 2 mm and power 100 watts. which is restated in Table 12. The center of the laser beam was located at (0.24595 m, 0.25 m, 0.2 m). The meshing technique used were similar to the one described earlier in Chapter 2. The results were used to predict the depth by using the equation (iii).

Name	Expression	Value	Description
r_spot	2 [mm]	0.002 m	Laser Diameter
emissivity	0.79	0.79	Emissivity of the Material
p_laser	100 [W]	100 W	Laser Power

Table.12. The Heat Source Used while Modelling Arbitrary Cracks

The time vs temperature plots for the arbitrary cracks are shown below.

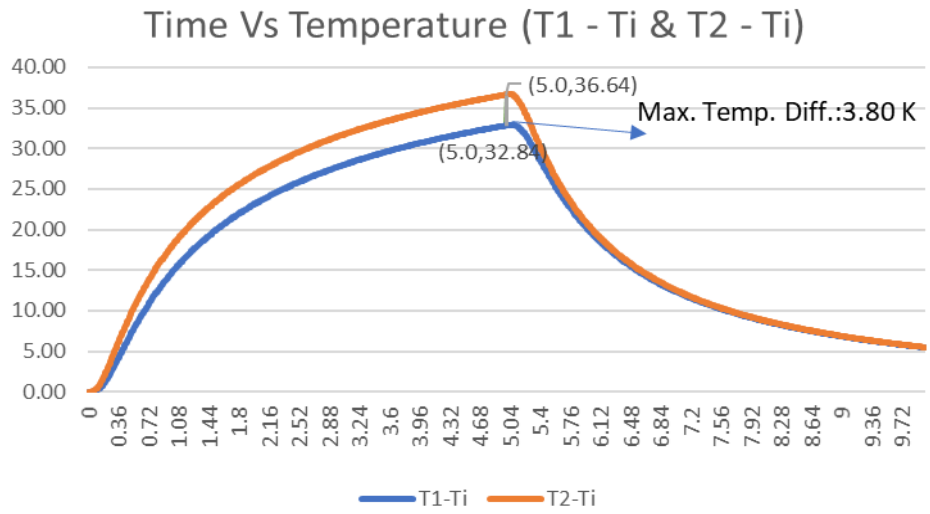

Figure 28. Time(t) vs Temperature (T1 - Ti & T2 - Ti) for Arbitrary Crack of Depth 0.7 mm

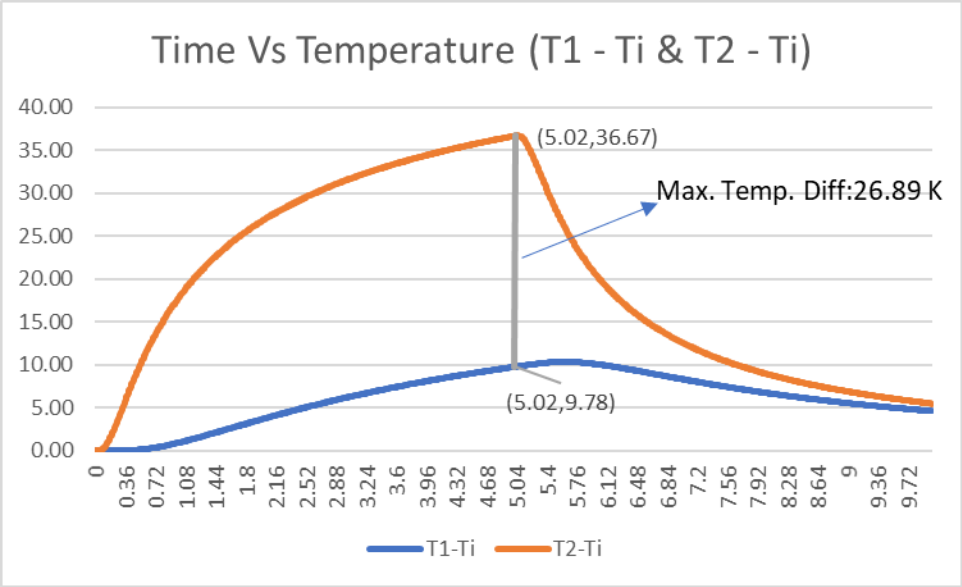

Figure 29. Time(t) vs Temperature (T1 - Ti & T2 - Ti) for Arbitrary Crack of Depth 3.8 mm

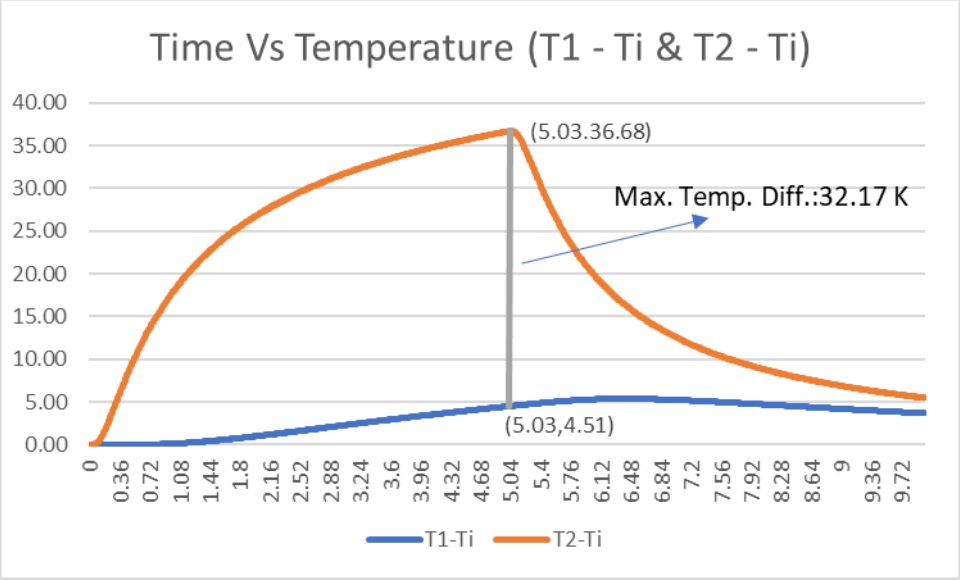

Figure 30. Time(t) vs Temperature (T1 - Ti & T2 - Ti) for Arbitrary Crack of Depth 5.5 mm

The equation to be used is restated below.

$y = 12.9873x^3 - 12.7914x^2 + 7.5291x + 0.058$

where,

x = Temperature differential index = ((T2(t')-Ti)-(T1(t')-Ti))/(T2(t')-Ti)

y = Predicted Depth of the Crack (rounded up to one decimal)

The predicted depths are tabulated below and compared with the actual depths.

X= ((T2(t')-Ti)-(T1(t')-Ti))/(T2(t')-Ti)	Predicted Depth (y)	Actual Depth(mm)	Error (mm)	Error %
0.1037	0.8	0.7	-0.1	14.29
0.7334	3.9	3.8	-0.1	2.63
0.8770	5.6	5.5	-0.1	1.82

Table.13. Predicted Depth and Actual Depth of Arbitrary Crack

Chapter 5: Conclusions

In this thesis, a three-dimensional modelling of laser point thermography with fifty cracks of different depth at the surface of the steel specimen was performed using COMSOL. The extracted data from the finite element analysis was then processed to best fit a polynomial curve and then regression analysis was performed. The equation obtained from the regression analysis was then used to predict the depth of the arbitrary cracks.

This thesis work used the modelling with the heat source which is nearest to the crack. Other locations of the laser incident point may also be feasible as long as maximum temperature difference is significant. The effect of change in heat source location on the regression equation is not studied in this work. Since the temperature difference is going to be different for new location of the heat source the coefficients of the regression equation are likely to change even if best fit curve would look similar.

It is worth mentioning that only the results from finite element modelling has been used in this thesis. Further work is needed to compare these results with the experimental results. Additionally, although very small, the radiation effect is not considered in the temperature differential. Furthermore, the data and hence the regression analysis presented here is based on the specimen material being steel. Hence the use of equation for predicting depth of crack in materials other than steel is not verified. Similar procedure may be followed in case of other materials, but another regression equation must be derived for predicting the depth of the crack.

This work is applicable for the cracks which are visible at the surface and propagate in a direction perpendicular to the surface. The applicability of this method for subsurface cracks is not verified. Furthermore, the crack is assumed to be long enough so that there is no heat propagated around the ends of the crack. Hence, the length of the crack does not necessarily have to be 0.5 m long as in the model. Similarly, the end boundaries of the specimen should not necessarily be located at the same distance from the source. The regression equation can be used as long as the heat does not propagate from the ends and the boundaries do not influence the heat flow.

In this work, the width of the crack is kept constant (0.1 mm). The regression curve is based on a specific set of heating parameters. Any change in the parameters will required a new regression analysis. The equation may change if the material of the specimen is changed since the heat conduction also depends on the material properties. Future works may be directed towards studying the effect on the temperature differential because of variations in the crack width, crack length, nearby boundary conditions, different material and laser power and laser pulse duration.

Appendix A

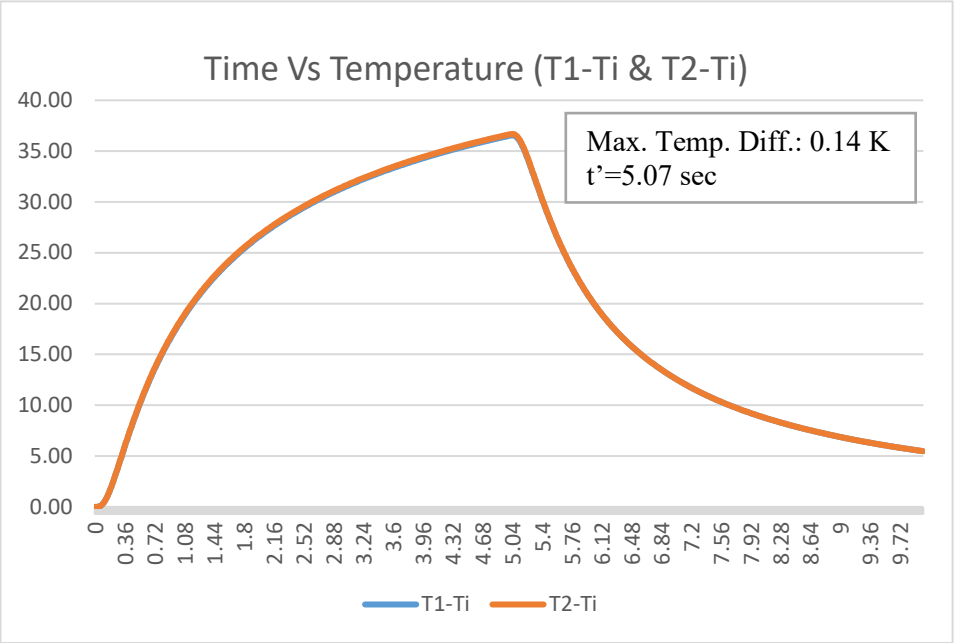

Figure A.1. Time(t) vs Temperature (T1 - Ti & T2 - Ti) for Crack Depth 0.1 mm

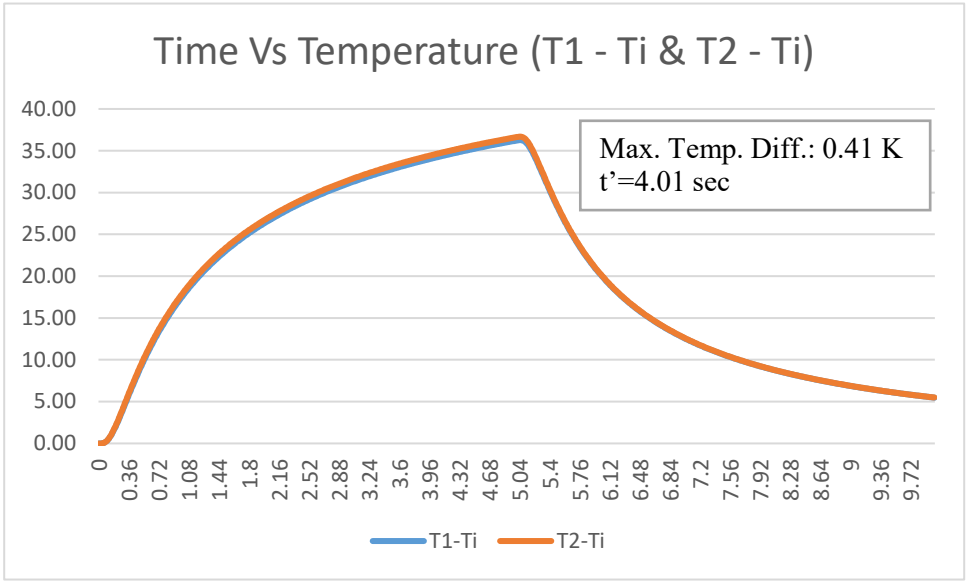

Figure A.2. Time(t) vs Temperature (T1 - Ti & T2 - Ti) for Crack Depth 0.2 mm

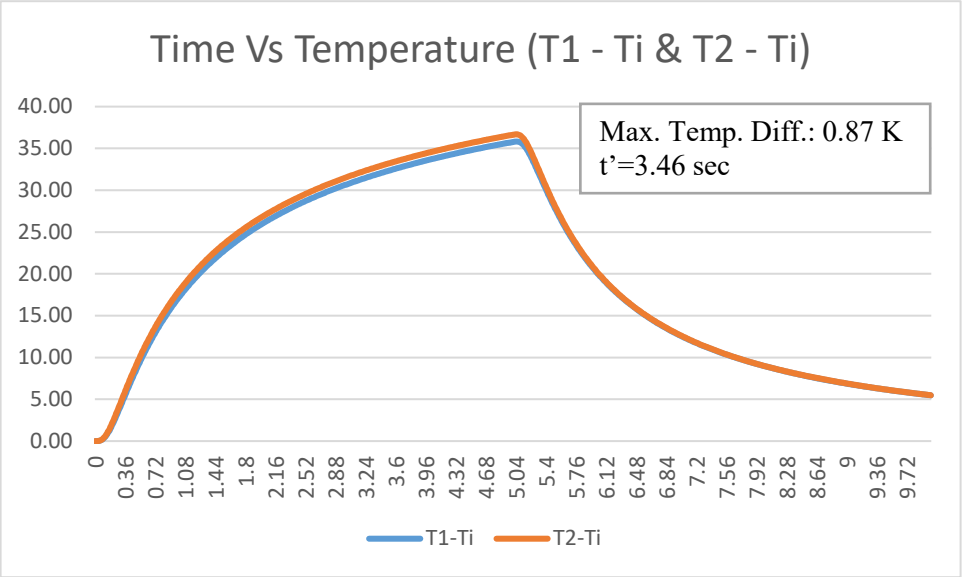

Figure A.3. Time(t) vs Temperature (T1 - Ti & T2 - Ti) for Crack Depth 0.3 mm

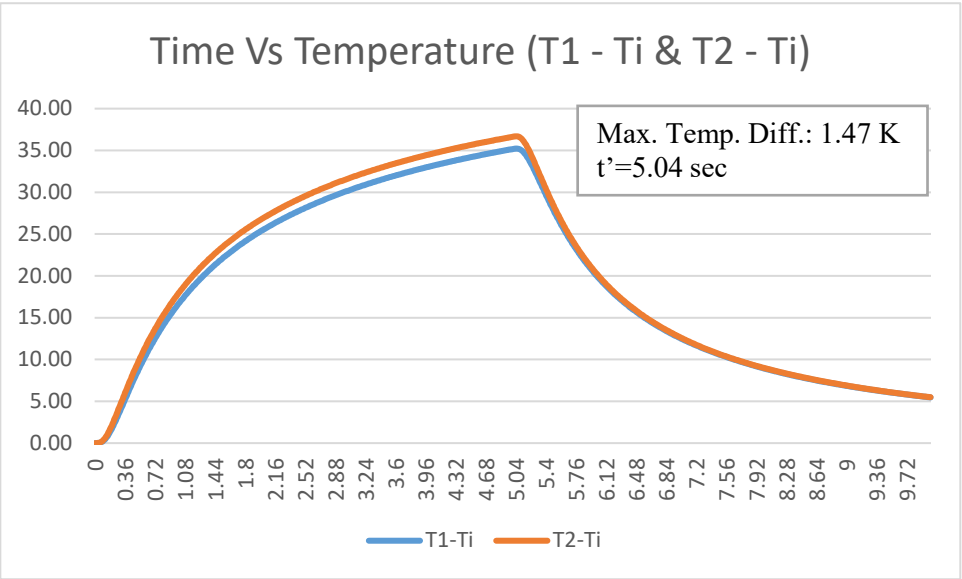

Figure A.4. Time(t) vs Temperature (T1 - Ti & T2 - Ti) for Crack Depth 0.4 mm

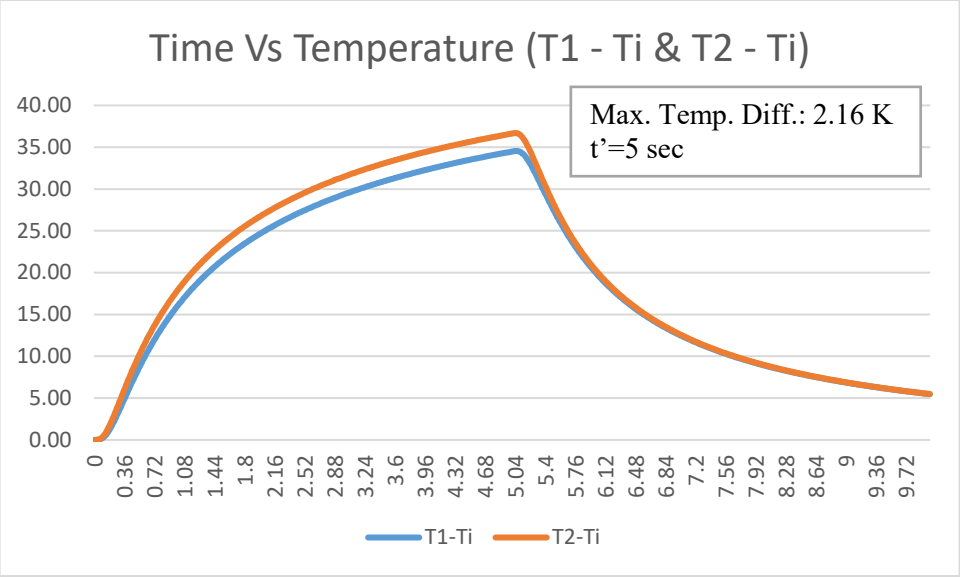

Figure A.5. Time(t) vs Temperature (T1 - Ti & T2 - Ti) for Crack Depth 0.5 mm

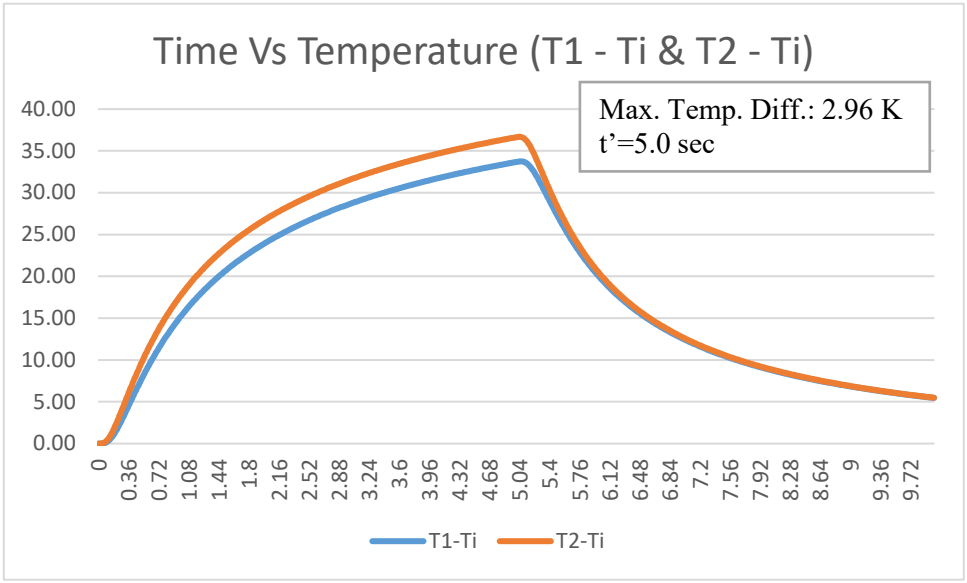

Figure A.6. Time(t) vs Temperature (T1 - Ti & T2 - Ti) for Crack Depth 0.6 mm

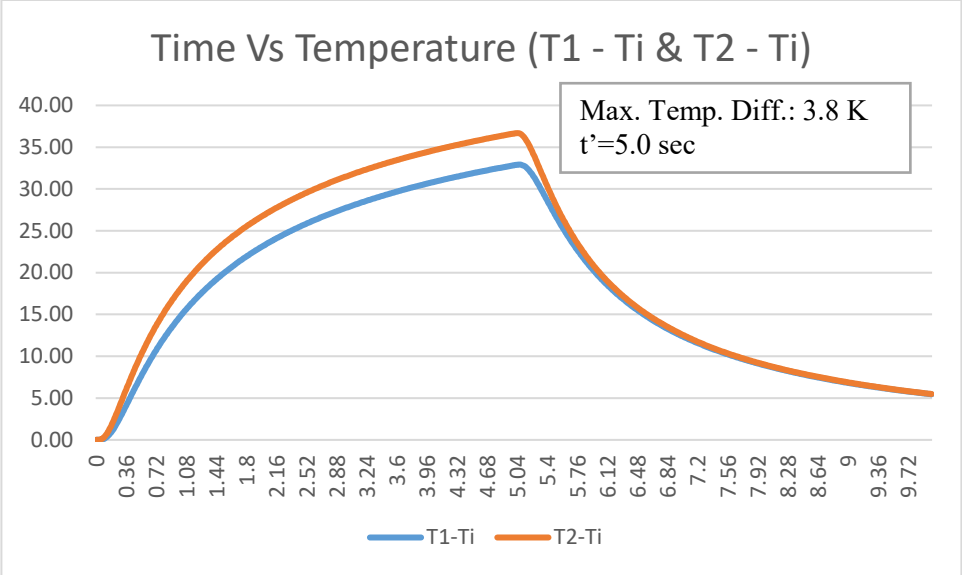

Figure A.7. Time(t) vs Temperature (T1 - Ti & T2 - Ti) for Crack Depth 0.7 mm (Arbitrary)

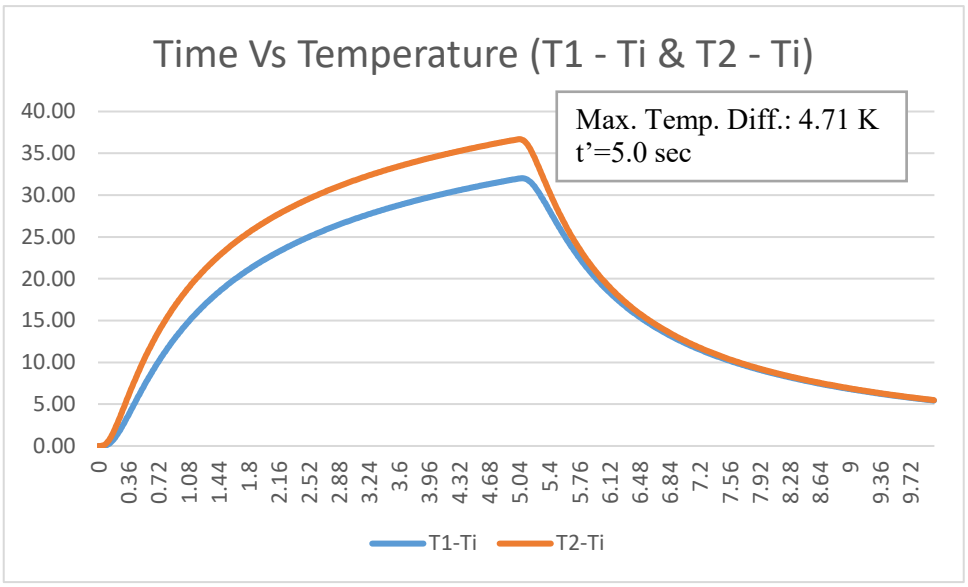

Figure A.8. Time(t) vs Temperature (T1 - Ti & T2 - Ti) for Crack Depth 0.8 mm

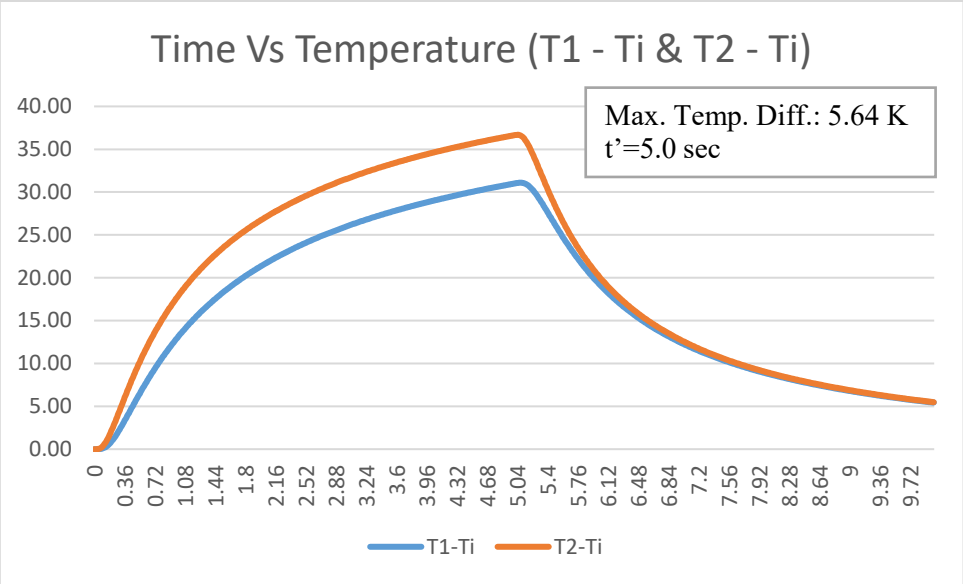

Figure A.9. Time(t) vs Temperature (T1 - Ti & T2 - Ti) for Crack Depth 0.9 mm

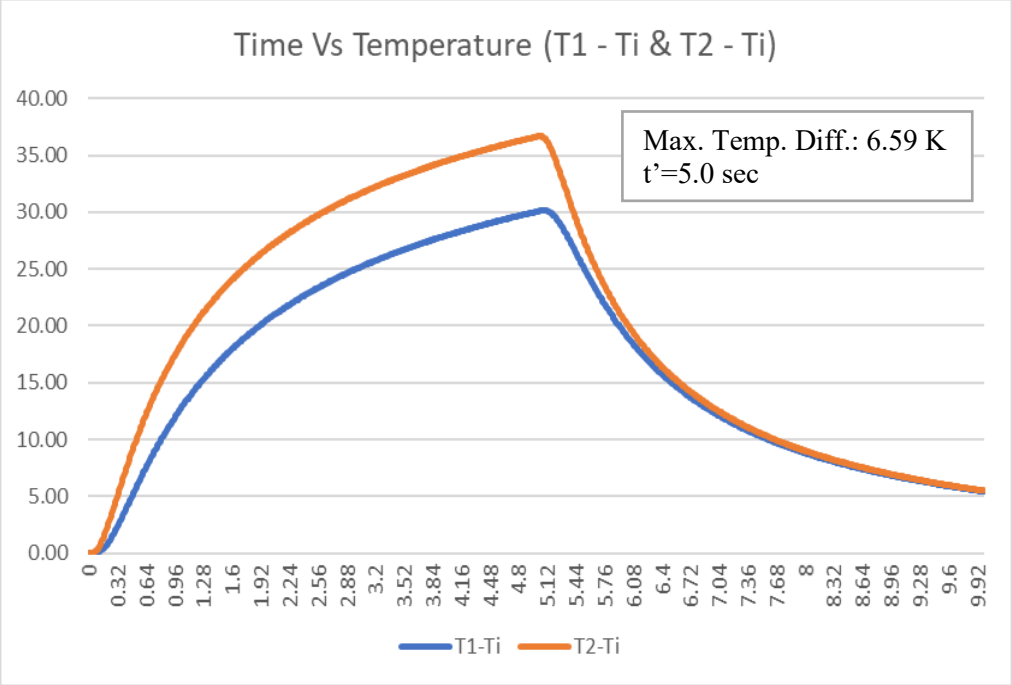

Figure A.10. Time(t) vs Temperature (T1 - Ti & T2 - Ti) for Crack Depth 1.0 mm

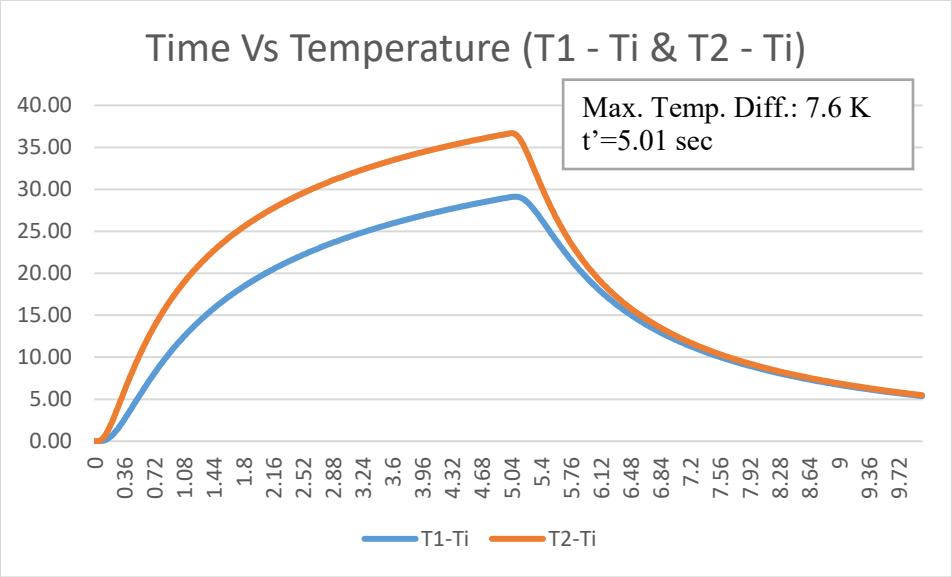

Figure A.11. Time(t) vs Temperature (T1 - Ti & T2 - Ti) for Crack Depth 1.1 mm

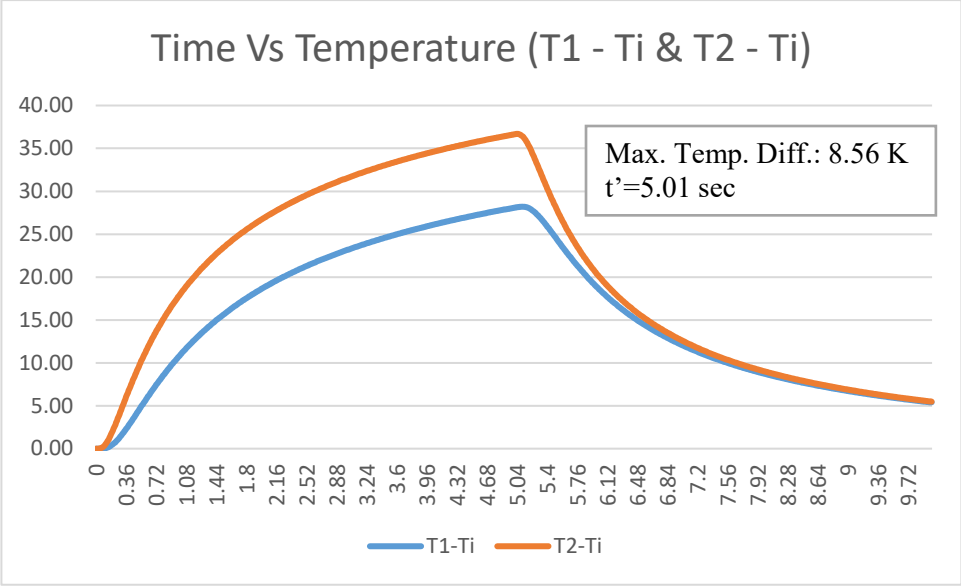

Figure A.12. Time(t) vs Temperature (T1 - Ti & T2 - Ti) for Crack Depth 1.2 mm

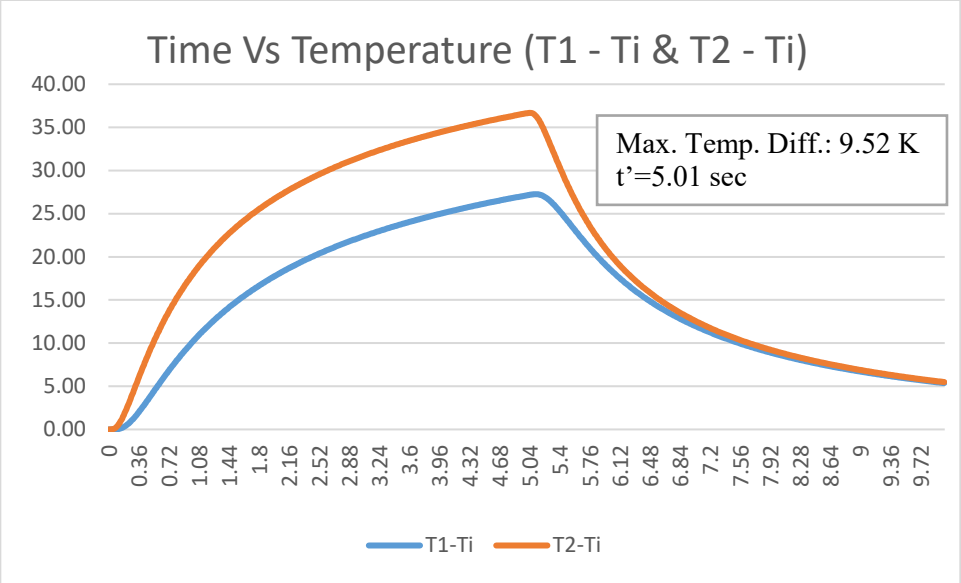

Figure A.13. Time(t) vs Temperature (T1 - Ti & T2 - Ti) for Crack Depth 1.3 mm

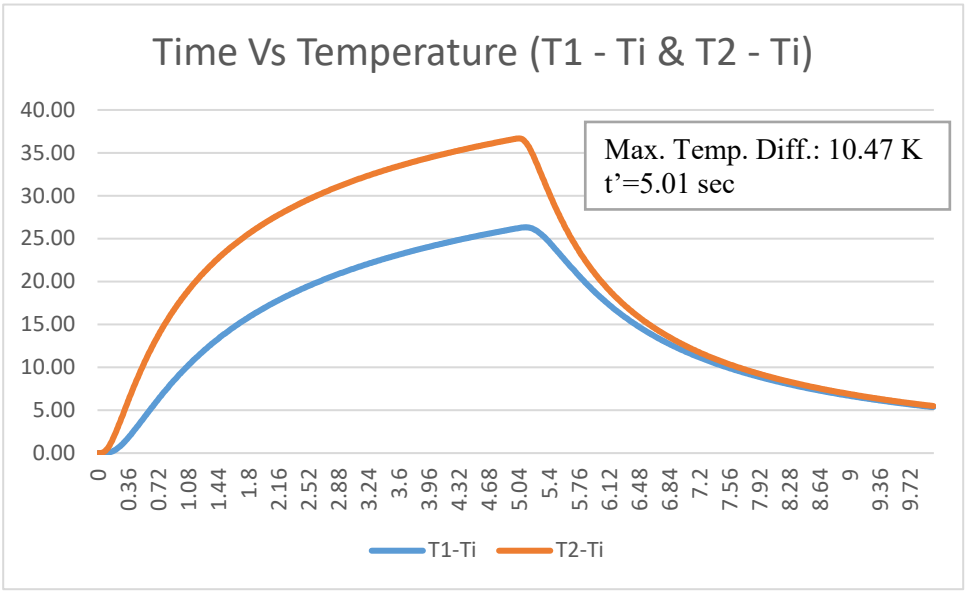

Figure A.14. Time(t) vs Temperature (T1 - Ti & T2 - Ti) for Crack Depth 1.4 mm

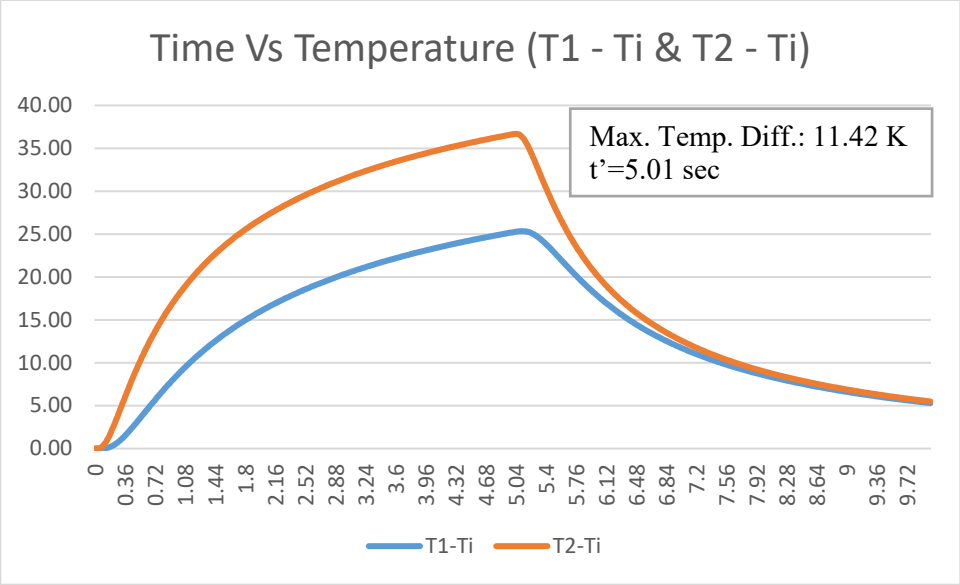

Figure A.15. Time(t) vs Temperature (T1 - Ti & T2 - Ti) for Crack Depth 1.5 mm

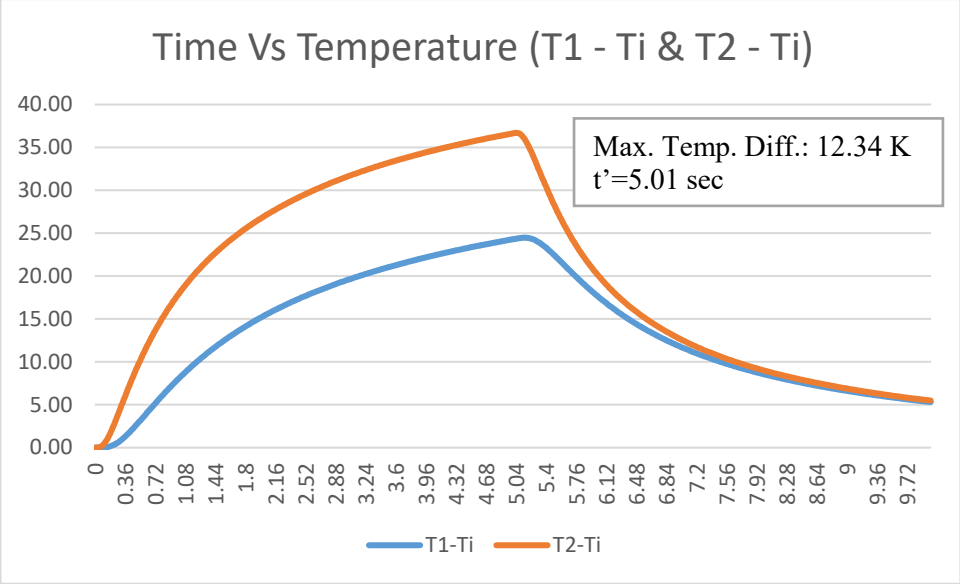

Figure A.16. Time(t) vs Temperature (T1 - Ti & T2 - Ti) for Crack Depth 1.6 mm

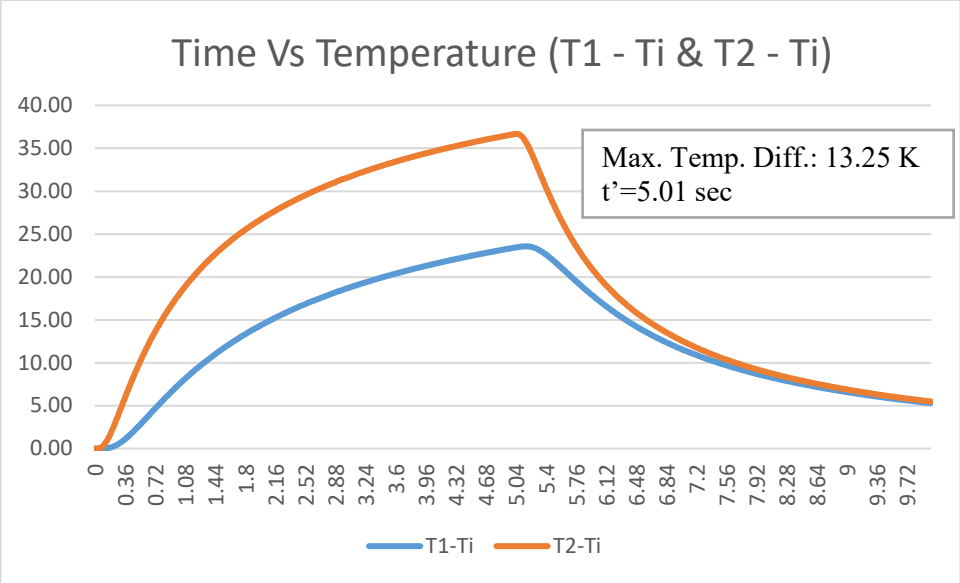

Figure A.17. Time(t) vs Temperature (T1 - Ti & T2 - Ti) for Crack Depth 1.7 mm

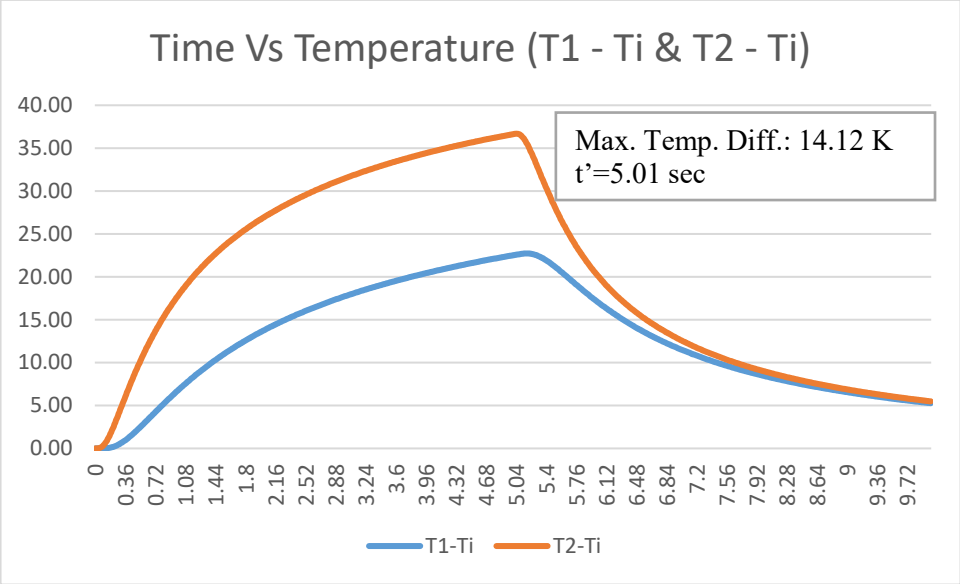

Figure A.18. Time(t) vs Temperature (T1 - Ti & T2 - Ti) for Crack Depth 1.8 mm

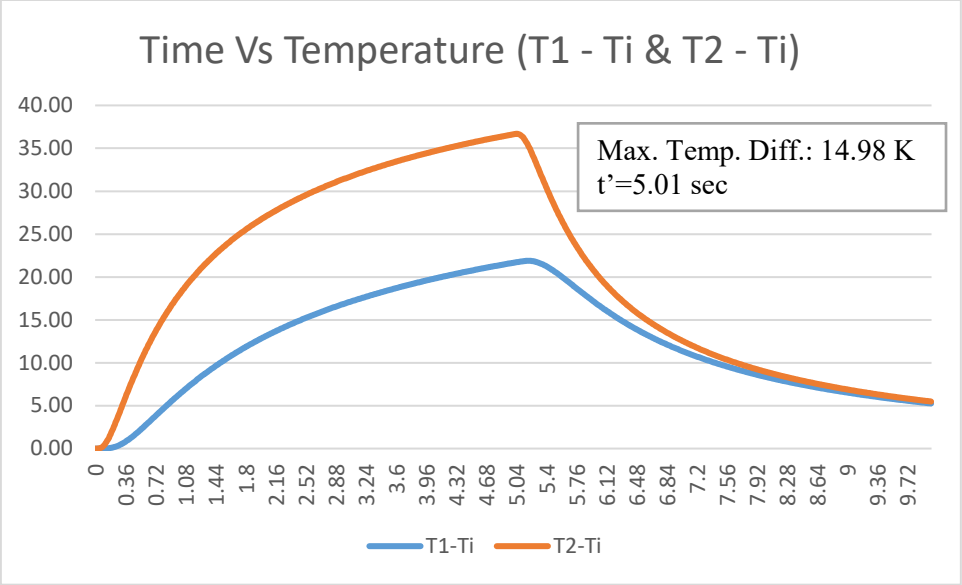

Figure A.19. Time(t) vs Temperature (T1 - Ti & T2 - Ti) for Crack Depth 1.9 mm

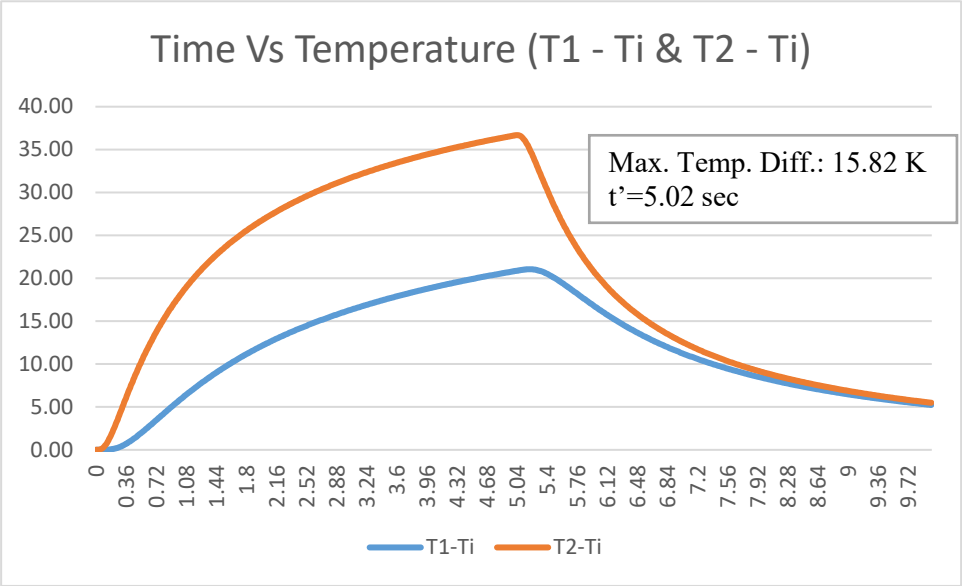

Figure A.20. Time(t) vs Temperature (T1 - Ti & T2 - Ti) for Crack Depth 2.0 mm

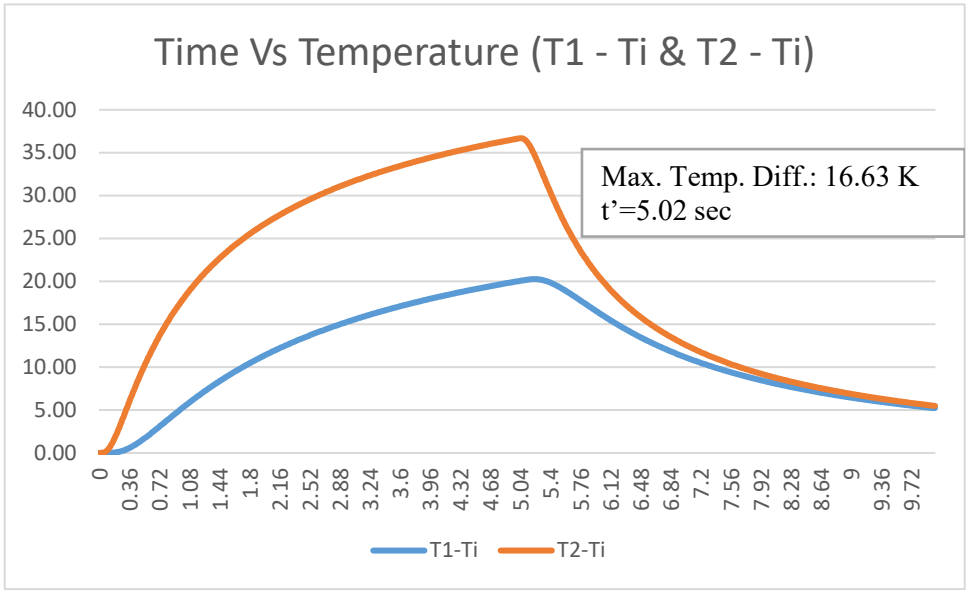

Figure A.21. Time(t) vs Temperature (T1 - Ti & T2 - Ti) for Crack Depth 2.1 mm

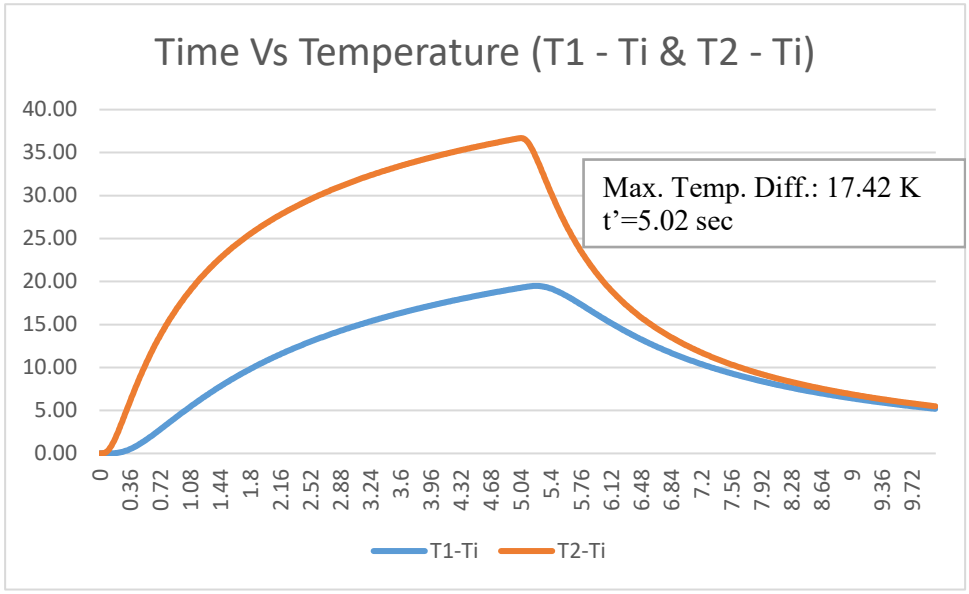

Figure A.22. Time(t) vs Temperature (T1 - Ti & T2 - Ti) for Crack Depth 2.2 mm

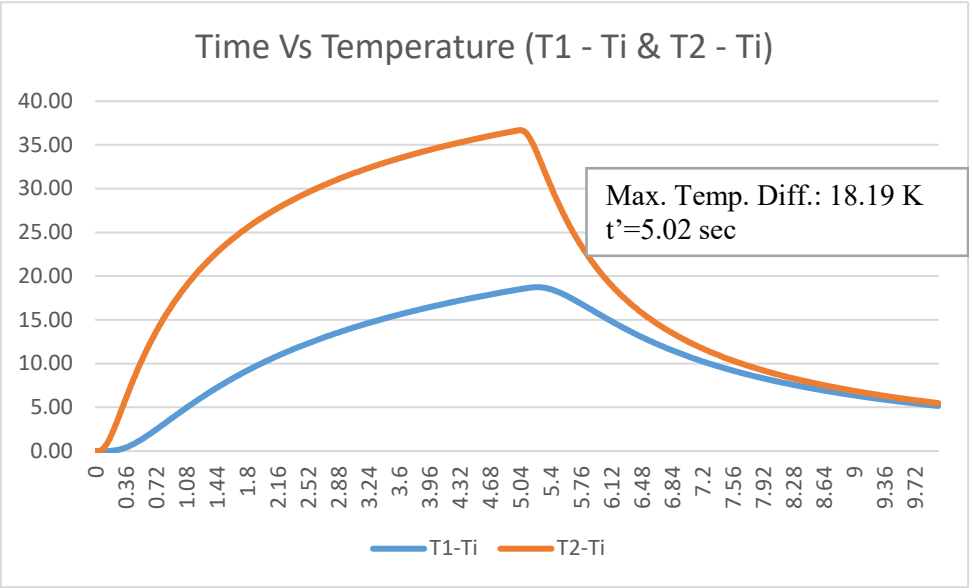

Figure A.23. Time(t) vs Temperature (T1 - Ti & T2 - Ti) for Crack Depth 2.3 mm

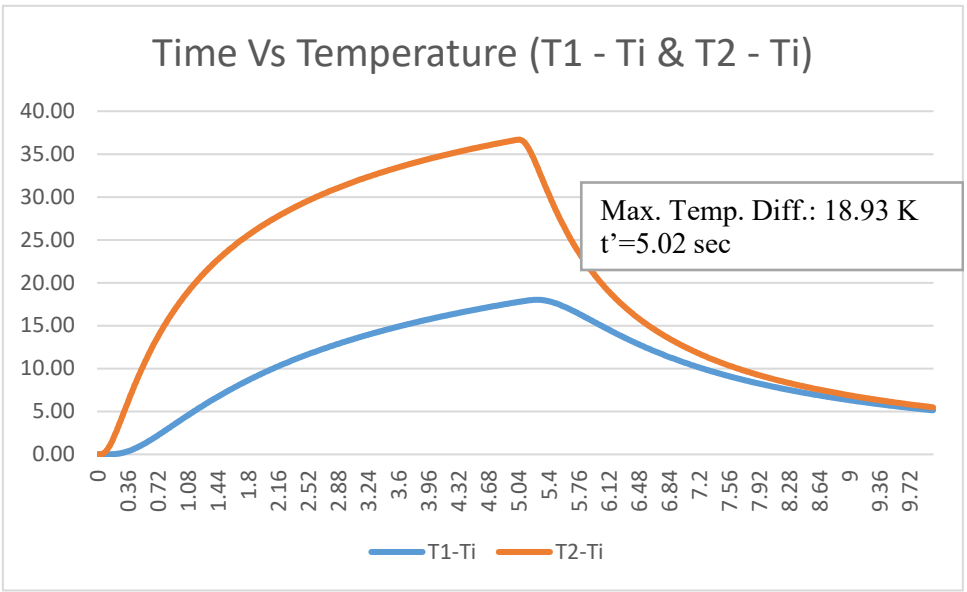

Figure A.24. Time(t) vs Temperature (T1 - Ti & T2 - Ti) for Crack Depth 2.4 mm

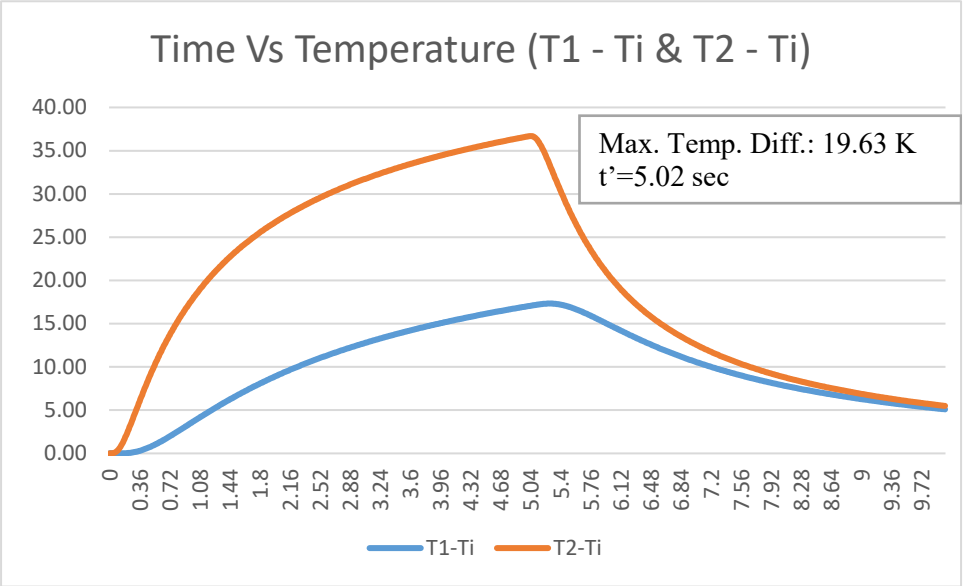

Figure A.25. Time(t) vs Temperature (T1 - Ti & T2 - Ti) for Crack Depth 2.5 mm

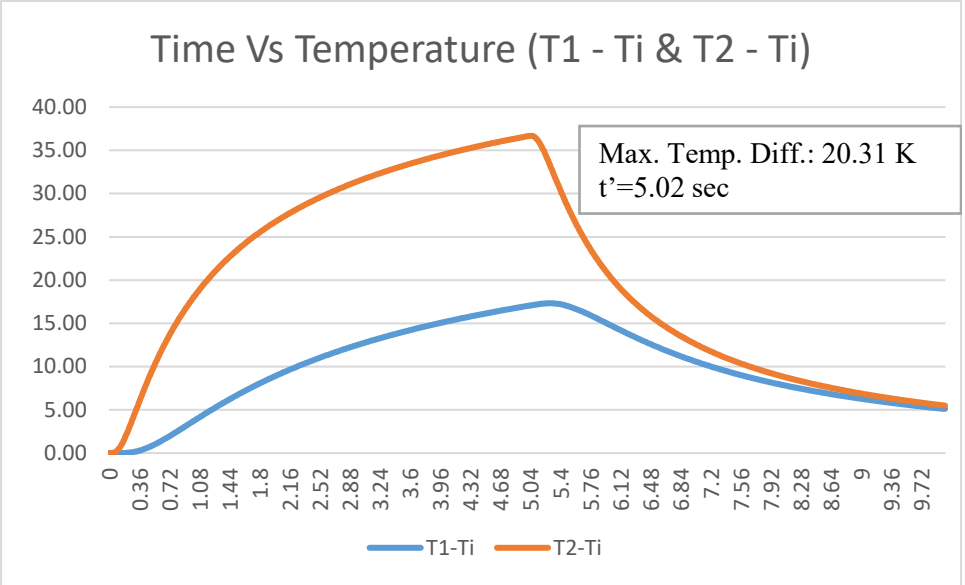

Figure A.26. Time(t) vs Temperature (T1 - Ti & T2 - Ti) for Crack Depth 2.6 mm

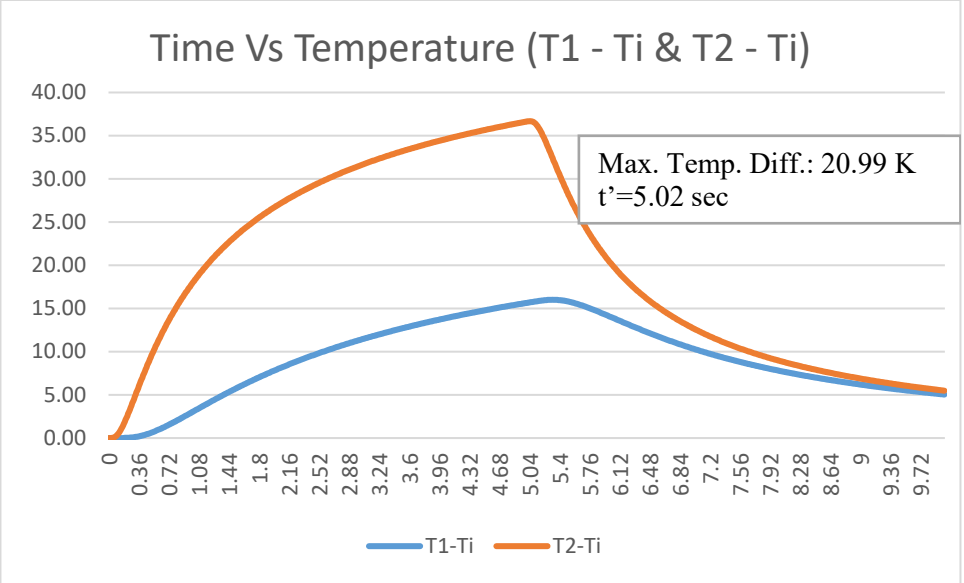

Figure A.27. Time(t) vs Temperature (T1 - Ti & T2 - Ti) for Crack Depth 2.7 mm

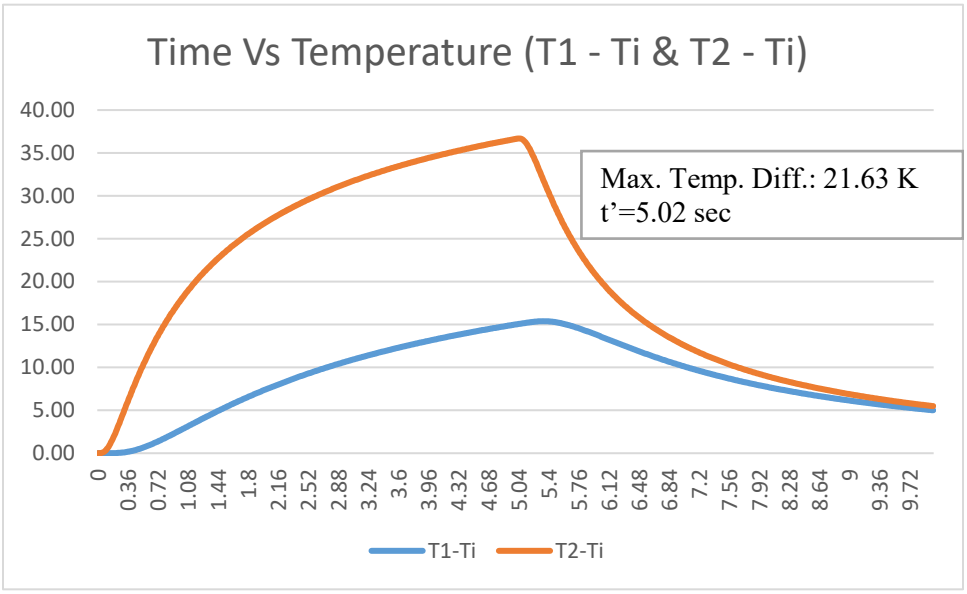

Figure A.28. Time(t) vs Temperature (T1 - Ti & T2 - Ti) for Crack Depth 2.8 mm

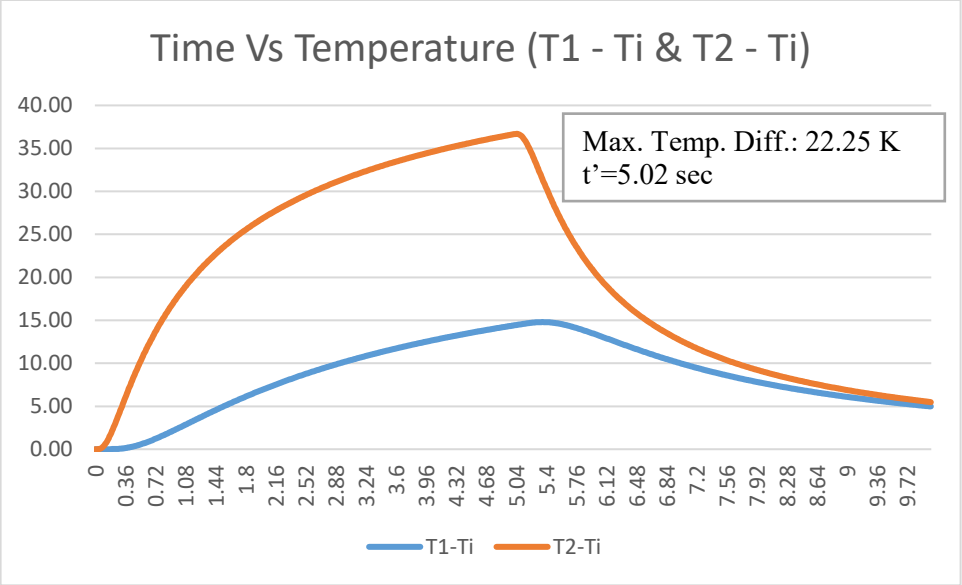

Figure A.29. Time(t) vs Temperature (T1 - Ti & T2 - Ti) for Crack Depth 2.9 mm

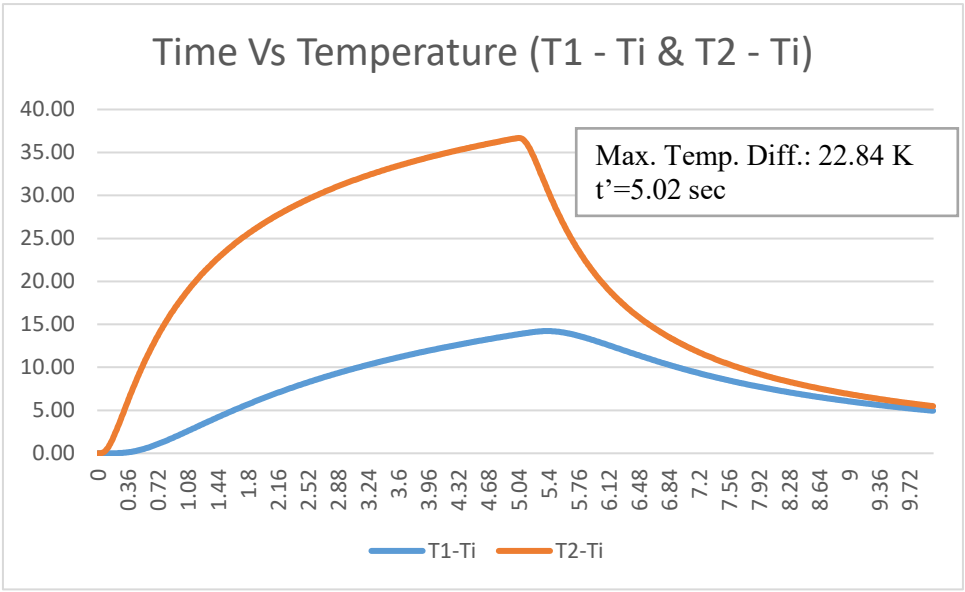

Figure A.30. Time(t) vs Temperature (T1 - Ti & T2 - Ti) for Crack Depth 3.0 mm

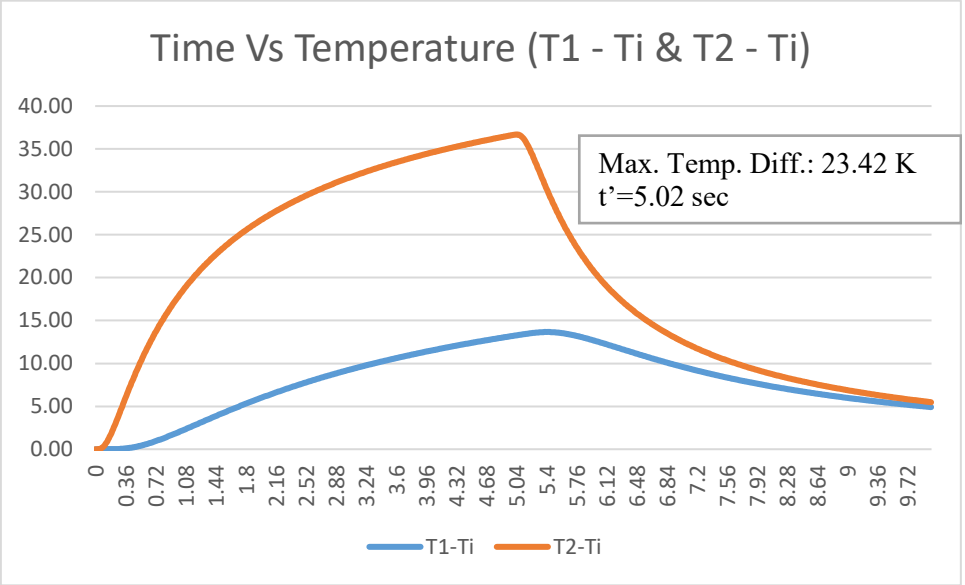

Figure A.31. Time(t) vs Temperature (T1 - Ti & T2 - Ti) for Crack Depth 3.1 mm

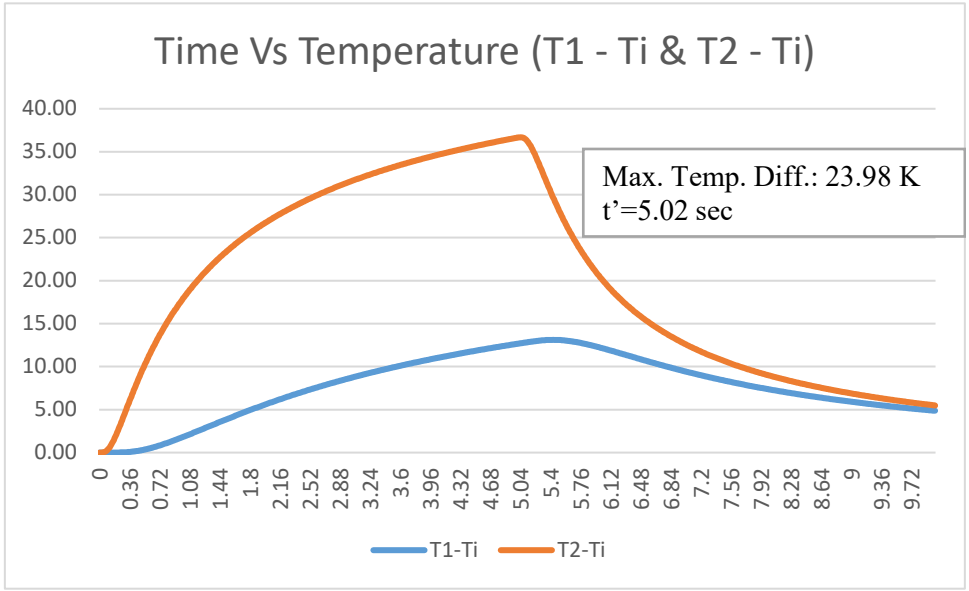

Figure A.32. Time(t) vs Temperature (T1 - Ti & T2 - Ti) for Crack Depth 3.2 mm

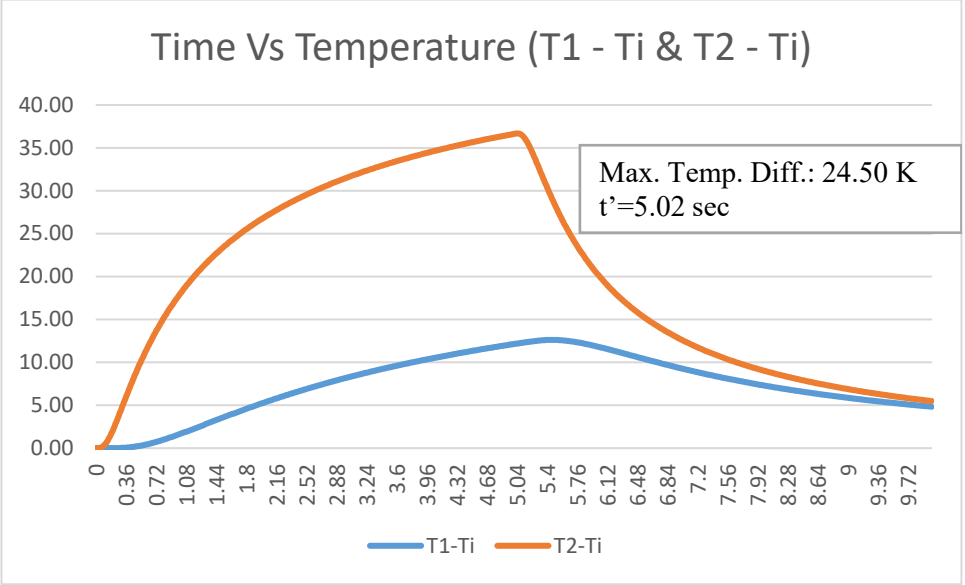

Figure A.33. Time(t) vs Temperature (T1 - Ti & T2 - Ti) for Crack Depth 3.3 mm

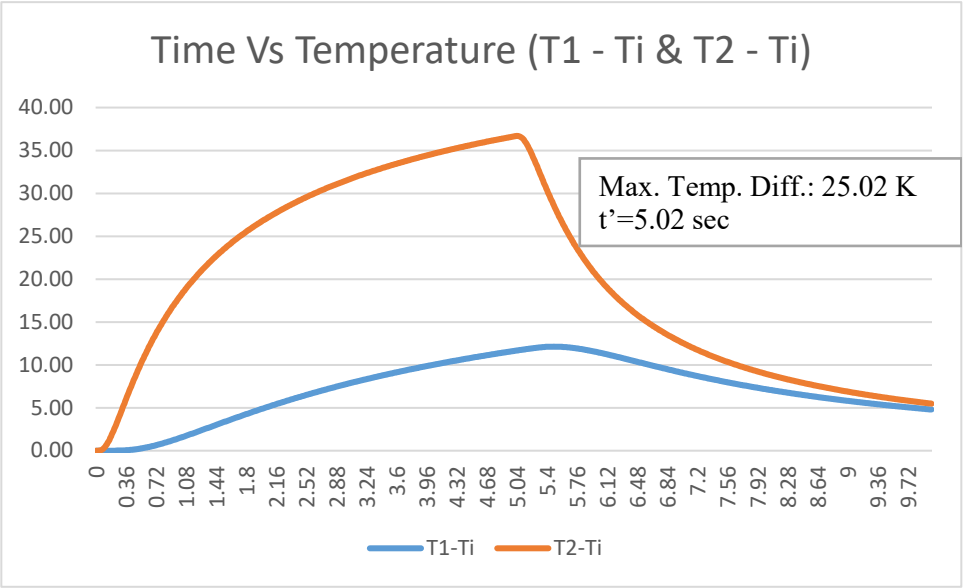

Figure A.34. Time(t) vs Temperature (T1 - Ti & T2 - Ti) for Crack Depth 3.4 mm

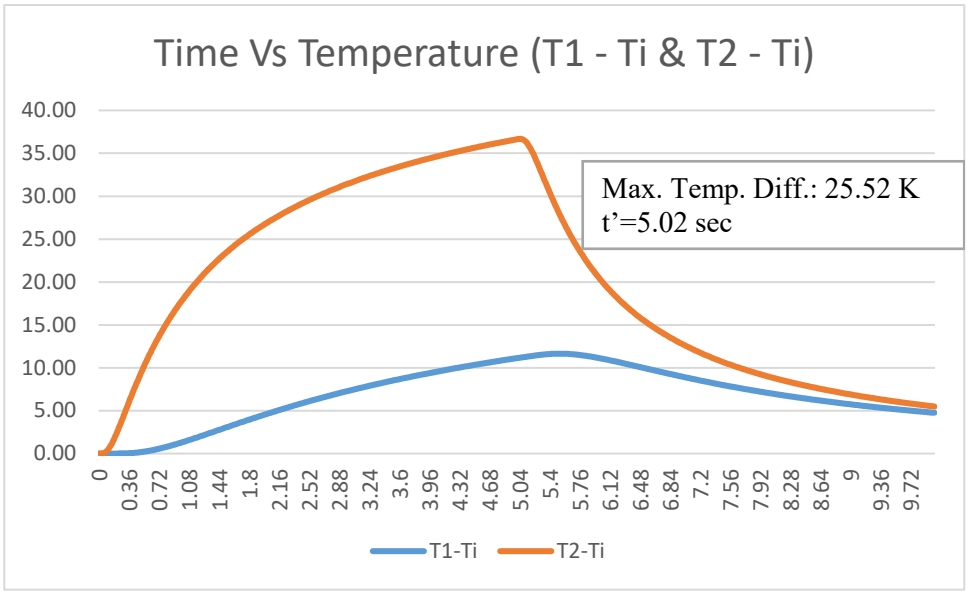

Figure A.35. Time(t) vs Temperature (T1 - Ti & T2 - Ti) for Crack Depth 3.5 mm

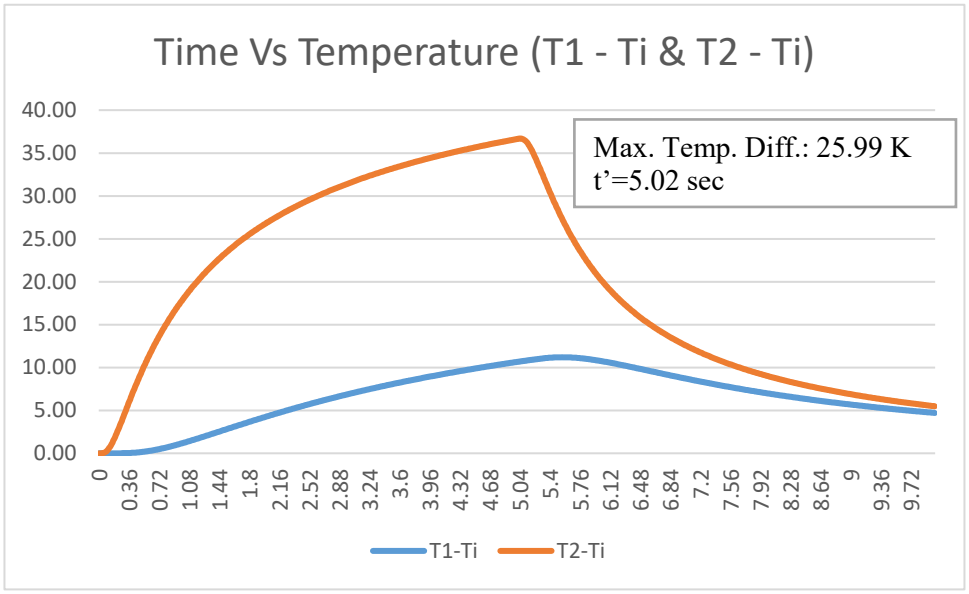

Figure A.36. Time(t) vs Temperature (T1 - Ti & T2 - Ti) for Crack Depth 3.6 mm

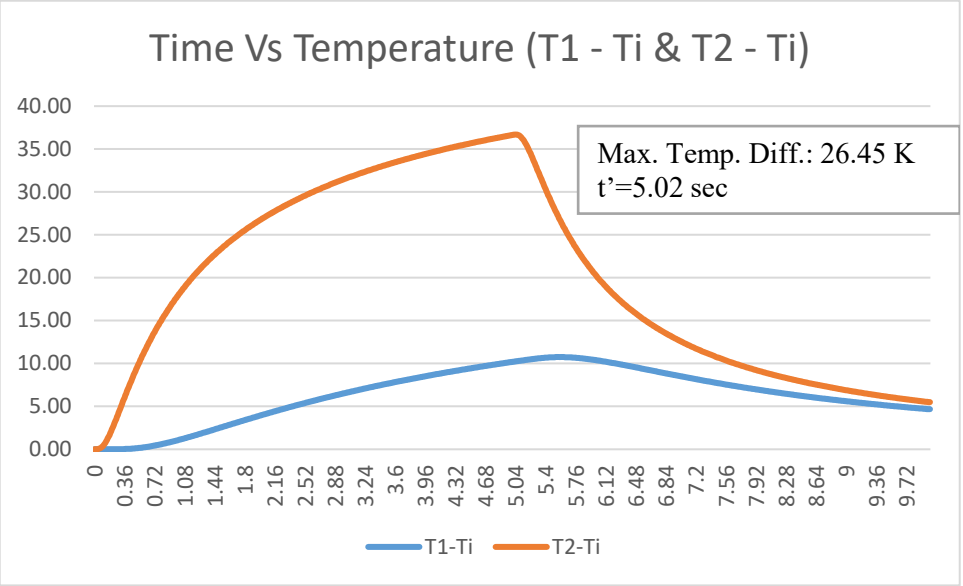

Figure A.37. Time(t) vs Temperature (T1 - Ti & T2 - Ti) for Crack Depth 3.7 mm

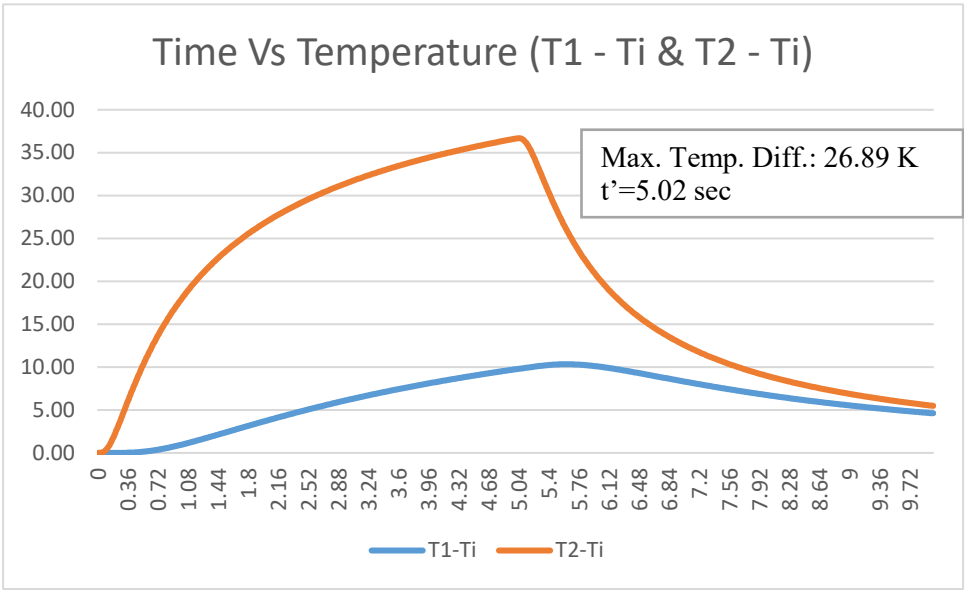

Figure A.38. Time(t) vs Temperature (T1 - Ti & T2 - Ti) for Crack Depth 3.8 mm (Arbitrary)

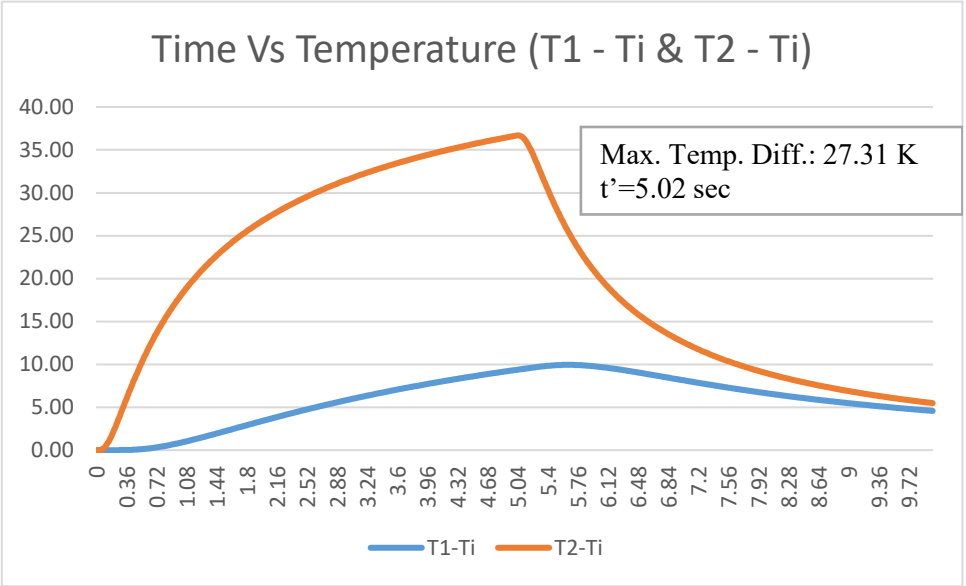

Figure A.39. Time(t) vs Temperature (T1 - Ti & T2 - Ti) for Crack Depth 3.9 mm

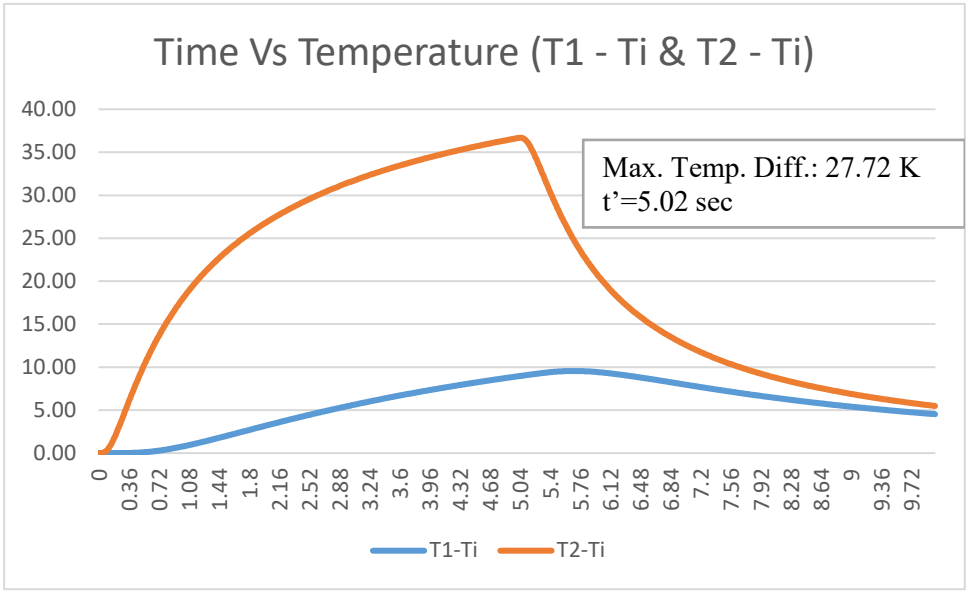

Figure A.40. Time(t) vs Temperature (T1 - Ti & T2 - Ti) for Crack Depth 4.0 mm

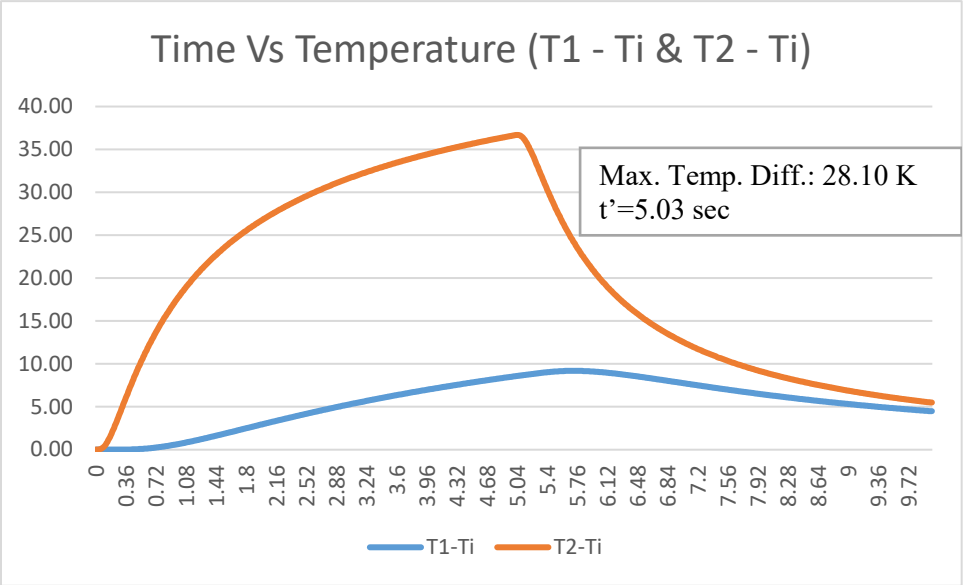

Figure A.41. Time(t) vs Temperature (T1 - Ti & T2 - Ti) for Crack Depth 4.1 mm

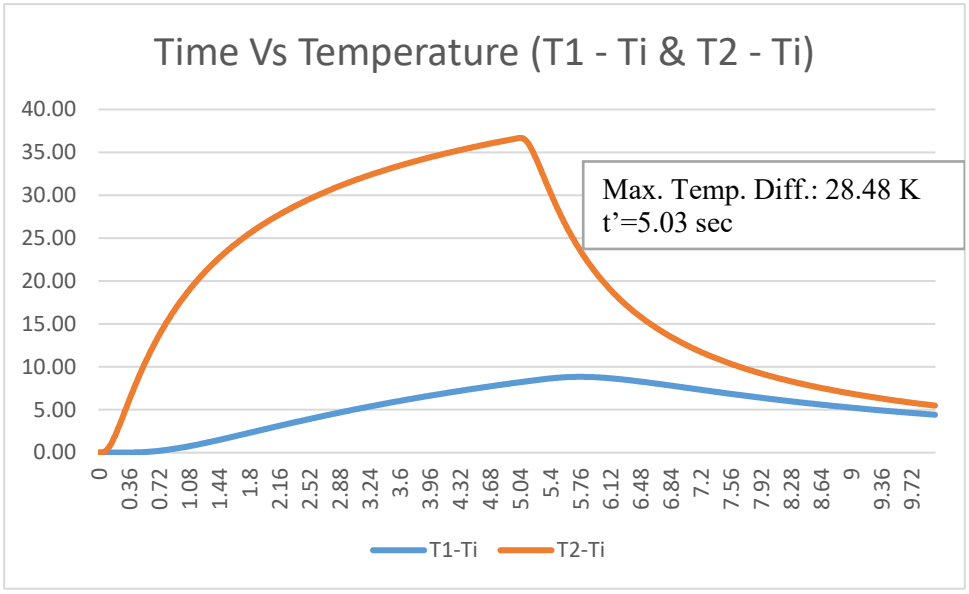

Figure A.42. Time(t) vs Temperature (T1 - Ti & T2 - Ti) for Crack Depth 4.2 mm

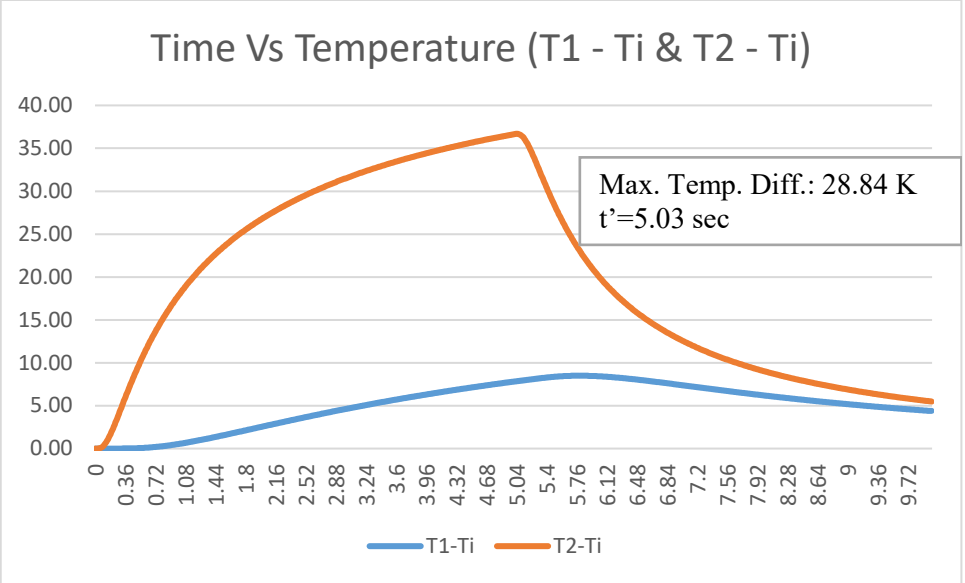

Figure A.43. Time(t) vs Temperature (T1 - Ti & T2 - Ti) for Crack Depth 4.3 mm

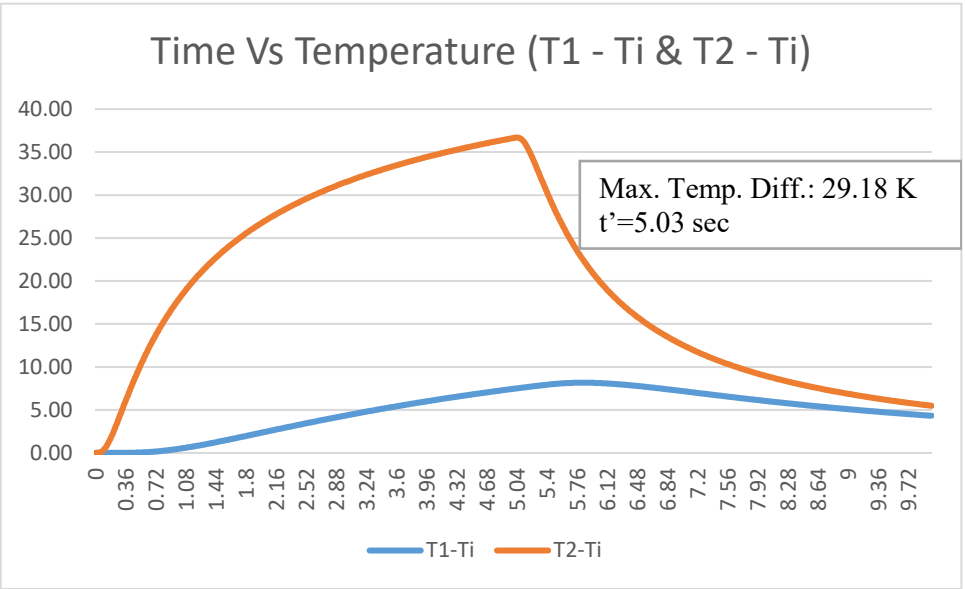

Figure A.44. Time(t) vs Temperature (T1 - Ti & T2 - Ti) for Crack Depth 4.4 mm

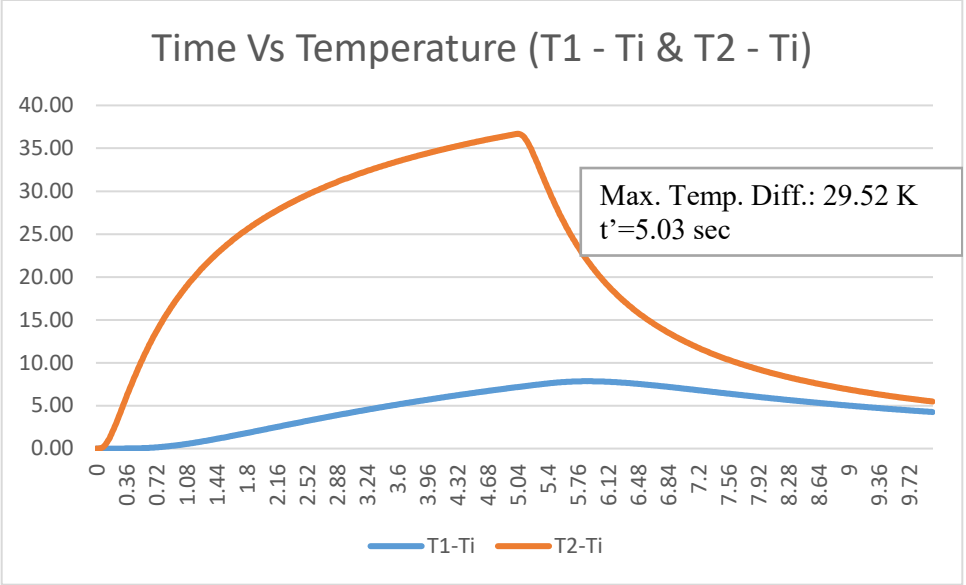

Figure A.45. Time(t) vs Temperature (T1 - Ti & T2 - Ti) for Crack Depth 4.5 mm

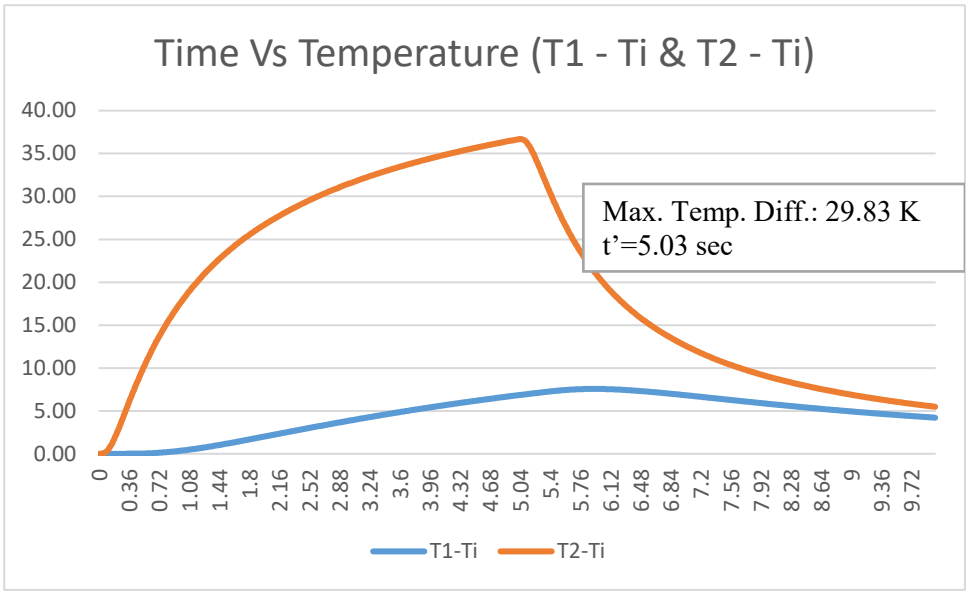

Figure A.46. Time(t) vs Temperature (T1 - Ti & T2 - Ti) for Crack Depth 4.6 mm

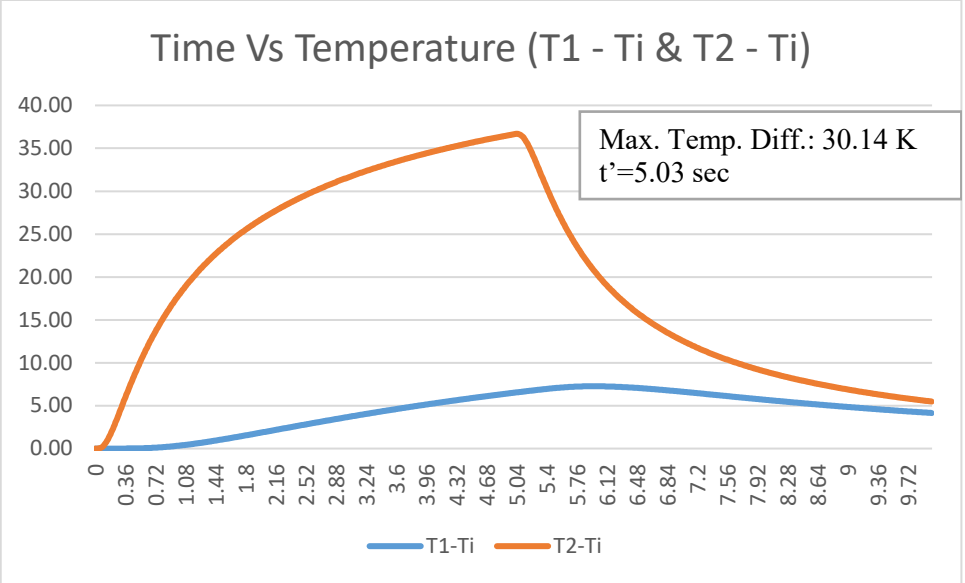

Figure A.47. Time(t) vs Temperature (T1 - Ti & T2 - Ti) for Crack Depth 4.7 mm

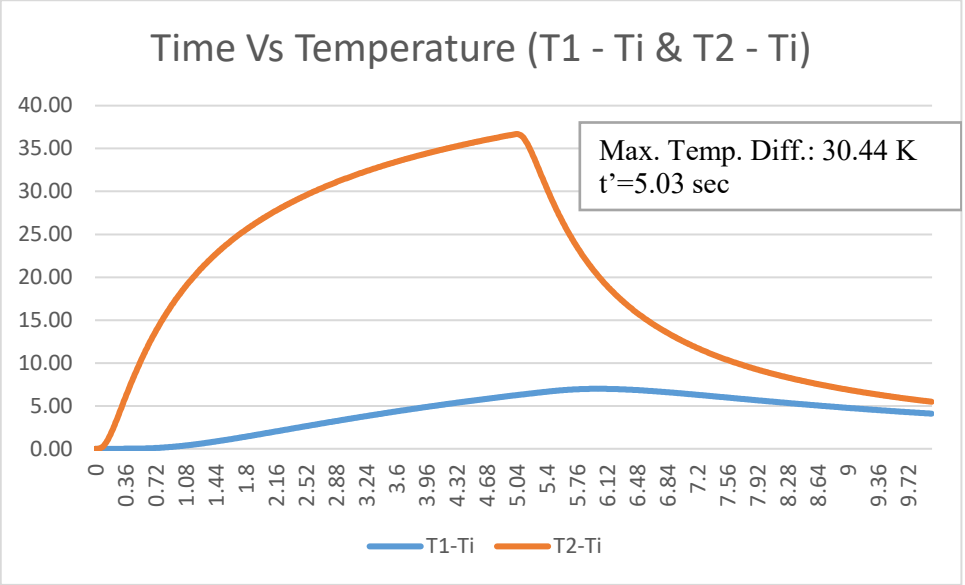

Figure A.48. Time(t) vs Temperature (T1 - Ti & T2 - Ti) for Crack Depth 4.8 mm

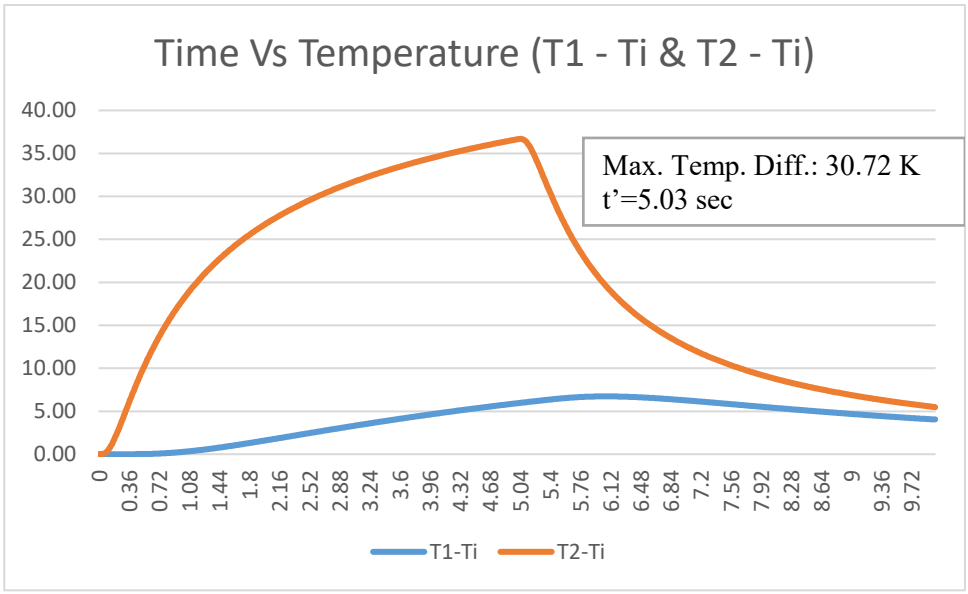

Figure A.49. Time(t) vs Temperature (T1 - Ti & T2 - Ti) for Crack Depth 4.9 mm

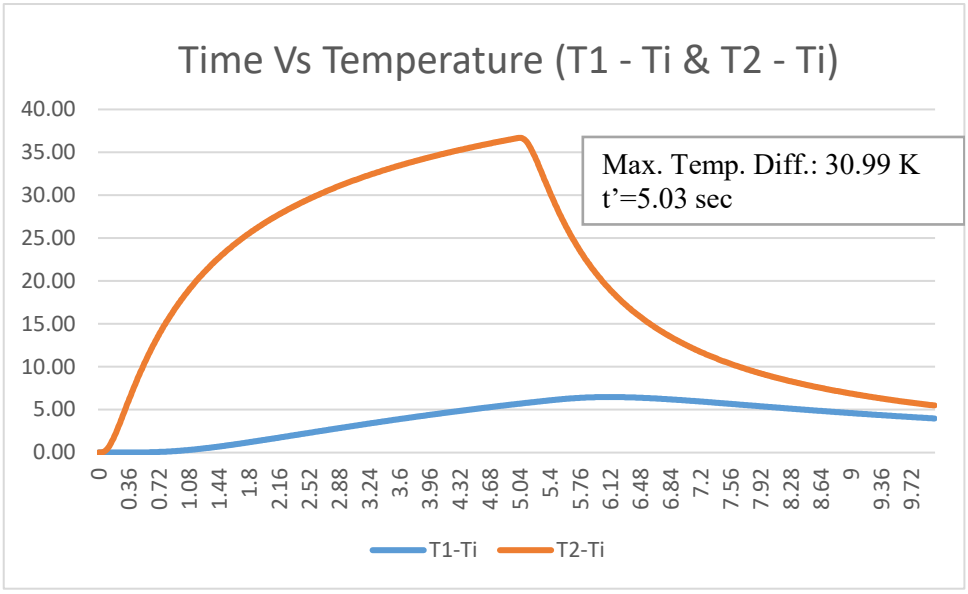

Figure A.50. Time(t) vs Temperature (T1 - Ti & T2 - Ti) for Crack Depth 5.0 mm

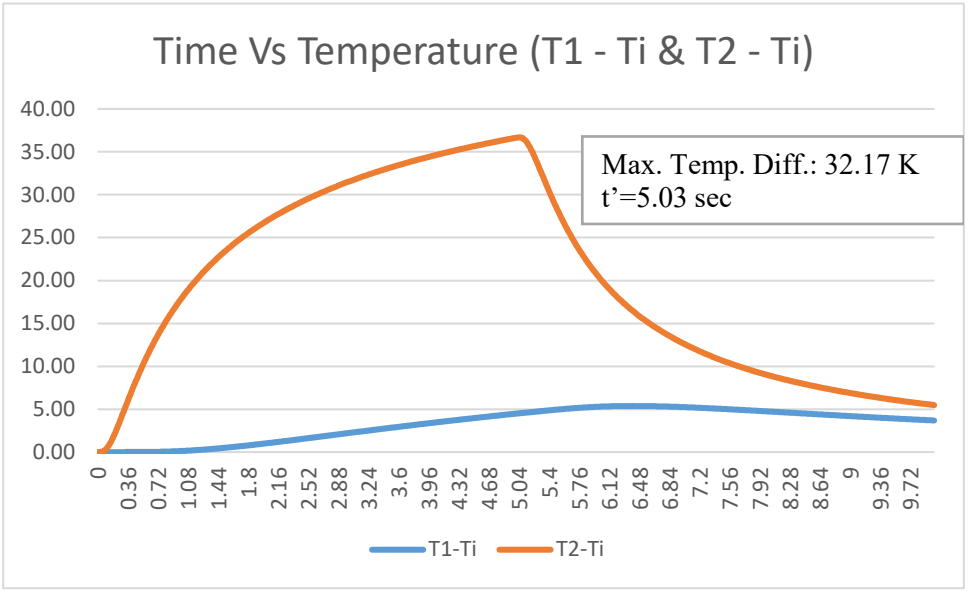

Figure A.51. Time(t) vs Temperature (T1 - Ti & T2 - Ti) for Crack Depth 5.5 mm

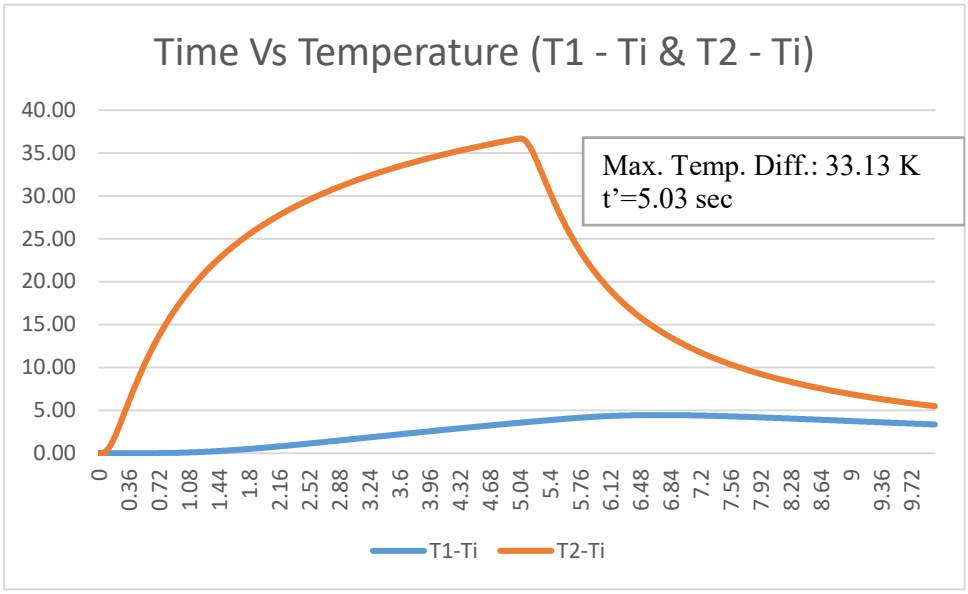

Figure A.52. Time(t) vs Temperature (T1 - Ti & T2 - Ti) for Crack Depth 6.0 mm

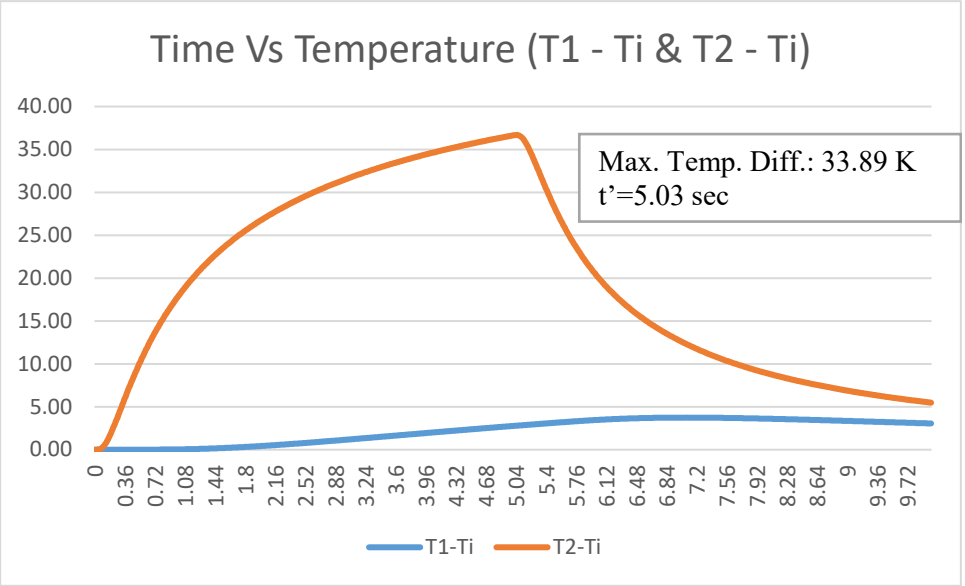

Figure A.53. Time(t) vs Temperature (T1 - Ti & T2 - Ti) for Crack Depth 6.5 mm

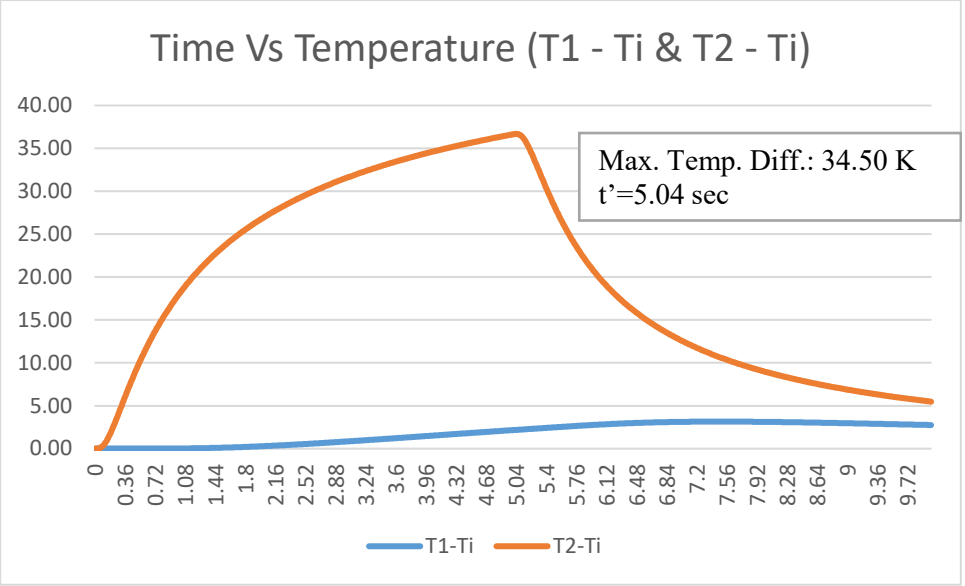

Figure A.54. Time(t) vs Temperature (T1 - Ti & T2 - Ti) for Crack Depth 7.0 mm

Appendix B

```
clear;
dat = xlsread('marchd.xlsx');
Tempr_Ratio = dat(:,2);
Depth = dat(:,1);
[p,s] = polyfit(Tempr_Ratio,Depth,3)
R_sq= 1 - (s.normr/norm(Depth - mean(Depth)))^2
Predicted_Depth = polyval(p,Tempr_Ratio);

plot(Tempr_Ratio,Depth,'o');
hold on
plot(Tempr_Ratio,Predicted_Depth);
hold off
xlabel('((T2(t`)-Ti)-(T1(t`)-Ti))/(T2(t`)-Ti)')
ylabel('Depth(mm)')
```

```
p =

   12.9873  -12.7914    7.5291    0.0580


s =

  struct with fields:

        R: [4×4 double]
       df: 50
    normr: 0.6346


R_sq =

    0.9974
```

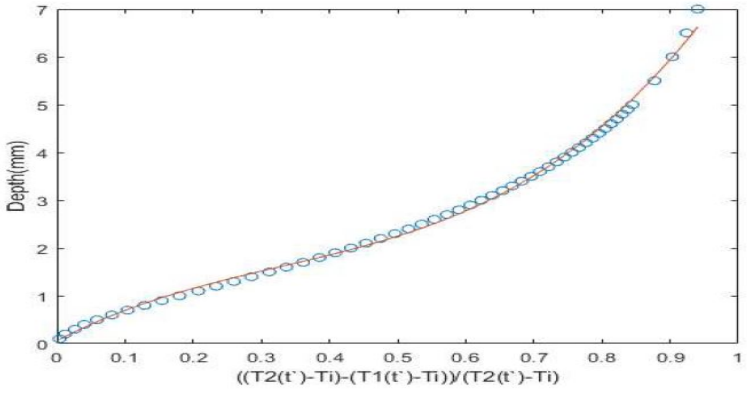

Published with MATLAB® R2019a

Bibliography

Aggelis, D. G., Kordatos, E. Z., Soulioti, D. V., & Matikas, T. E. (2010). Combined use of thermography and ultrasound for the characterization of subsurface cracks in concrete. *Construction and Building Materials*, *24*(10), 1888–1897. https://doi.org/10.1016/j.conbuildmat.2010.04.014

Avdelidis, N. P., Gan, T.-H., Ibarra-Castanedo, C., & Maldague, X. P. V. (2011). Infrared thermography as a nondestructive tool for materials characterisation and assessment. *Thermosense: Thermal Infrared Applications XXXIII*, *8013*, 801313. https://doi.org/10.1117/12.887403

Azizinamini, A., Power, E. H., Myers, G. F., Ozyildirim, H. C., Kline, E. S., Whitmore, D. W., & Mertz, D. R. (2013). Design Guide for Bridges for Service Life. In *Design Guide for Bridges for Service Life*. Transportation Research Board. https://doi.org/10.17226/22617

Basheer, M., Pv, N., Ravindran, P., & Balasubramaniam, K. (2015). A thermographic approach for surface crack depth evaluation through 3D finite element modeling. *AIP Conference Proceedings*, *1650*(April), 1782–1789. https://doi.org/10.1063/1.4914802

Burrows, S. E., Dixon, S., Pickering, S. G., Li, T., & Almond, D. P. (2011). *Thermographic detection of surface breaking defects using a scanning laser source*. https://doi.org/10.1016/j.ndteint.2011.06.001

COMSOL Multiphysics. (2015). Heat Transfer Module. *Manual*, 1–222.

Frei, W. (2015a, March). *Improving Your Meshing with Partitioning | COMSOL Blog*. https://www.comsol.com/blogs/improving-your-meshing-with-partitioning/

Frei, W. (2015b, June). *Modeling Laser-Material Interactions in COMSOL Multiphysics | COMSOL Blog*. https://www.comsol.com/blogs/modeling-laser-material-interactions-in-comsol-multiphysics/

Introduction to Nondestructive Testing. (n.d.). Retrieved March 27, 2020, from https://www.asnt.org/MajorSiteSections/About/Introduction_to_Nondestructive_Testing.aspx

Jung, J. Y., Yoon, H. J., & Cho, H. W. (2018). A Study on Crack Depth Measurement in Steel Structures Using Image-Based Intensity Differences. *Advances in Civil Engineering*, *2018*. https://doi.org/10.1155/2018/7530943

Laser Heating of a Silicon Wafer. (n.d.). Retrieved March 27, 2020, from https://www.comsol.com/model/laser-heating-of-a-silicon-wafer-13835

Li, T., Almond, D. P., & Rees, D. A. S. (2011). Crack imaging by scanning laser line

thermography. *AIP Conference Proceedings*, *1335*(June), 407–414. https://doi.org/10.1063/1.3591881

Li, T., Almond, D. P., Rees, D. A. S., Weekes, B., & Pickering, S. G. (2010). Pulsed laser spot imaging thermography, modelling and experimental data. *AIP Conference Proceedings*, *1211*(1), 435–442. https://doi.org/10.1063/1.3362426

Maldague, X. P. V. (2002). Introduction to NDT by active infrared thermography. *Materials Evaluation*, *60*(9), 1060–1073.

Rashed, A., Almond, D. P., Rees, D. A. S., Burrows, S., & Dixon, S. (2007). Crack detection by laser spot imaging thermography. *AIP Conference Proceedings*, *894*, 500–506. https://doi.org/10.1063/1.2718013

Schlichting, J., Kervalishvili, G. N., Maierhofer, C., & Kreutzbruck, M. (2010). Imaging cracks by laser excited thermography. *AIP Conference Proceedings*, *1211*(March), 727–734. https://doi.org/10.1063/1.3362466

Schlichting, Joachim, Ziegler, M., Maierhofer, C., & Kreutzbruck, M. (2012). Flying Laser Spot Thermography for the Fast Detection of Surface Breaking Cracks. *18th World Conference on Nondestructive Testing*, *April*, 7.